

1 2 9 0



UNIVERSIDADE DE
COIMBRA

Marina Oliva

**3D PRINTED STRUCTURES WITH
TUNABLE WETTABILITIES**

VOLUME 1

Dissertação no âmbito do Mestrado em Engenharia de Materiais, orientada pela Professora Doutora Ana Paula da Fonseca Piedade e pelo Doutor Akel Ferreira Kanaan e apresentada ao Departamento de Engenharia Mecânica da Faculdade de Ciências e Tecnologia da Universidade de Coimbra.

October 2021

1 2 9 0



UNIVERSIDADE D
COIMBRA

3D PRINTED STRUCTURES WITH TUNABLE WETTABILITIES

Submitted in Partial Fulfilment of the Requirements for the Degree of Master in
Material Engineering.

ESTRUTURAS 3D IMPRESSAS COM MOLHABILIDADE AJUSTÁVEL

Author

Marina Piasentini Oliva

Advisors

Professora Doutora Ana Paula da Fonseca Piedade

Doutor Akel Ferreira Kanaan

Jury

President	Doutora Patrícia Freitas Rodrigues Investigadora doutorada da Universidade de Coimbra
Vowel	Doutora Ana Catarina da Silva Pinho Investigadora doutorada da Universidade de Coimbra
Advisor	Doutor Akel Ferreira Kanaan Bolsheiro de Investigação da Universidade de Coimbra

The work was partially financed by the Add.Additive project – Additive Manufacturing to Portuguese Industry, co-financed by the European Regional Development Fund (ERDF), through the Portugal-2020 program (PT2020), under the Incentive System for Research and Technological Development (SI I&DT), and by the Competitiveness and Internationalization Operational Program (POCI-01-0247-FEDER-024533).



UNIÃO EUROPEIA
Fundo Europeu
de Desenvolvimento Regional

Coimbra, October, 2021

Nothing in life is to be feared, it is only to be understood. Now is the time to
understand more, so that we may fear less.

Marie Currie, 1903.

To my parents.

ACKNOWLEDGEMENTS

I have received a great deal of support and assistance as well as encouragement and patience throughout the duration of this project

I would first like to thank my supervisors, PhD Ana Paula da Fonseca Piedade and PhD Akel Kanaan, whose expertise was invaluable in provided me with the tools that I needed to choose the right direction and successfully complete my dissertation. Your insightful feedback and constructive criticism pushed me to sharpen my thinking and brought my work to a higher level.

I would like to acknowledge my colleagues from my Master at University of Coimbra for their helpful advice and unwavering support.

I would also like to extend my deepest gratitude to my parents and sister for their wise counsel and profound belief in my abilities. You are always there for me. Finally, the completion of my dissertation would not have been possible without the support and nurturing of my friends, Marcela Saspadini and Mariana Cheles, who provided inspiration and motivation as well as happy distractions to rest my mind outside of my research.

ABSTRACT

Mineral-based waste oils are a current environmental problem due to the lack of simple methods that allow their separation from water and subsequent recycling.

This work aims to study the influence of geometry and roughness on the wettability of printed objects obtained by FFF (Fused filament fabrication) technology, using as polymers FOMM[®]-60 and HIPS (high impact polystyrene). Therefore, the objective is to create a physical separation system for water/oil dispersions, without the use of surfactants.

Porosity and surface roughness were studied from the perspective of their influence on the hydrophobicity of the samples and, consequently, on the separation capacity of the constituents of oil/water emulsions. Additionally, the influence of the geometry of the printed sample (pyramid or semi-sphere) was analyzed, as well as the chemistry of the material used.

The specimens printed with HIPS exhibit a hydrophobic character, while those made of FOMM[®]-60 are hydrophilic. In addition, the FOMM[®]-60 samples of pyramidal geometry and permeable membrane with triangular infill are the components that potentially benefit the separation process, as they have a greater interaction with oil and water, when compared to the semi-sphere geometry and with the pyramidal geometry in HIPS.

In the future, a separation column with several layers of the printed components with better performance should be made, to assess their real effectiveness in the process of separating oil/water emulsions. If effective, this procedure will allow a sustainable way to clean water.

Keywords 3D printing, Oil/water separation, Hydrophobicity, Wettability, Geometry.

RESUMO

Os óleos residuais de base mineral são um problema ambiental atual devido à falta de métodos simples que permitam a sua separação da água e posterior reciclagem.

Este trabalho tem como objetivo estudar a influência da geometria e da rugosidade na molhabilidade de objetos impressos obtidos pela tecnologia FFF (Fused filament fabrication), utilizando os polímeros FOMM[®]-60 e HIPS (poliestireno de elevado impacto). Deste modo, o objetivo é criar um sistema de separação física de dispersões água/óleo sem a utilização de surfactantes.

A porosidade e a rugosidade superficiais foram estudadas na perspectiva da sua influência na hidrofobicidade das amostras e, conseqüentemente, na capacidade de separação dos constituintes das emulsões óleo/água. Adicionalmente, foi analisada a influência da geometria da amostra impressa (pirâmide ou semiesfera), bem como da química do material utilizado.

Os provetes impressos com HIPS exibem um caráter hidrófobo, enquanto os constituídos por FOMM[®]-60 são hidrófilos. Além disso, as amostras de FOMM[®]-60 de geometria piramidal e membrana permeável com preenchimento triangular são os componentes que potencialmente beneficiam o processo de separação, uma vez que possuem uma maior interação com o óleo e água, quando comparados com a geometria de semiesfera e com a geometria piramidal em HIPS.

No futuro deverá ser efetuada uma coluna com várias camadas dos componentes com melhor desempenho para aferir da sua real eficácia no processo de separação das emulsões óleo/água.

Palavras chave: Impressão 3D, Óleo-água separação, Hidrofobicidade, Molhabilidade, Geometria.

Contents

LIST OF FIGURES	ix
LIST OF TABLES	xi
LIST OF SIMBOLS AND ACRONYMS/ ABBREVIATIONS.....	xiii
List of Symbols.....	xiii
Acronyms/Abbreviations.....	xiii
Introduction	1
1. State of the art.....	3
1.1. Oil/water suspension, emulsion and the environmental problem.....	3
1.2. Suspension / emulsion separation process	7
1.3. Suspension / emulsion separation technology by physical processes.....	9
1.4. Suspension / emulsion separation by hierarchical roughness and surface properties	11
2. Work Project.....	14
2.1. Motivation.....	14
2.2. Material Processing - 3D Printing	14
2.3. Materials	16
3. Materials and Methods	18
3.1. Material.....	18
3.2. 3D Printing.....	18
3.3. Characterization Techniques.....	19
3.3.1. Fourier Transform Infrared Spectroscopy (FTIR).....	19
3.3.2. Thermogravimetry Analysis (TGA)	19
3.3.3. Differential Scanning Calorimetry (DSC).....	19
3.3.4. Scanning electron microscopy (SEM).....	20
3.3.5. Water-swelling test.....	20
3.3.6. Contact angle	21
3.3.7. Slippery drop test (oil and water)	21
3.4. Printing pattern	22
4. Results and discussion	24
4.1. 3D samples.....	24
4.2. Chemical characterization.....	26
4.2.1. FTIR	26
4.2.2. Water swelling test	28
4.3. Thermal analysis	30
4.4. Morphological analysis.....	34
4.5. Wetting of the printed samples	35
4.5.1. Geometrical samples.....	35
4.5.2. Permeable membrane samples.....	44
CONCLUSIONS AND Future WORK.....	48
BIBLIOGRAPHY	51

APPENDIX A – DSC ANALYSES RESULTS FOR FOMM[®]-60 FILAMENTS 56

LIST OF FIGURES

Figure 1.1 – Laboratory assembly liquid–liquid extraction (9).....	4
Figure 1.2 – Diagram illustrating the demulsification of oil-in-water emulsion process with a MRGO noncompound (11).....	5
Figure 1.3 – Mechanical separation of oil and water by microfiltration process (14).	6
Figure 1.4 – Interaction between surfactants and molecules as the critical micelle formation concentration (CMC) is developed (18).....	7
Figure 1.5 – SEM images of a hydrophobic plant (A) <i>Nelumbo nucifera</i> (lotus flower) (31).	11
Figure 1.6 – “Salvinia effect “(a) eggbeater shaped surface morphology (b) “petal effect” of the eggbeater shaped topography (25).	12
Figure 1.7 – Top view of the patterns chosen for the microstructures. The white regions correspond to a high plane and the gray regions to a low plane. Where (a) square, (b) round e (c) hexagon.	13
Figure 2.1 - Schematic of FFF adapted from (39).....	15
Figure 2.2 - Schematic diagram of (a) (b) nozzle flow and (c) (d) horizontal turn (38).	16
Figure 2.3 – High impact polystyrene chemical structure (43).	17
Figure 2.4 – Chemistry of the unit structures of (A) PVA (47) and (B) TPU (48).	17
Figure 4.1 – FTIR spectrum of HIPS filaments.	26
Figure 4.2 – FTIR spectrum of FOMM [®] -60 filaments before and after the soaking process, normalized by the most intense peak of each spectrum, respectively 1734 cm ⁻¹ and 0,08 cm ⁻¹	27
Figure 4.3 – The water uptake capacity of the FOMM [®] -60 and HIPS printed samples.	29
Figure 4.4 – Thermogravimetric and TGA derivative (DTG) profiles of HIPS.....	30
Figure 4.5 – Thermogravimetric and TGA derivative (DTG) profiles of FOMM [®] -60.....	30
Figure 4.6 – DSC thermograms for HIPS sample with exothermal events oriented up.....	32
Figure 4.7 –DSC thermograms for FOMM [®] -60 sample with exothermal events oriented up.	33
Figure 4.8 - SEM micrographs of FOMM [®] -60 samples after and before washing procedures.	35
Figure 4.9– Sample’s interaction with a drop of water during the contact angle test. A) Pyramidal HIPS DQ sample B) Half sphere HIPS DQ sample.	36
Figure 4.10 – Pyramidal samples contact angle measurement with water (■, ■, ■) and oil (■, ■, ■) as the drop’s content.	37
Figure 4.11 – Contact angle measurement with water and oil as the drop’s content in pyramidal (■, ■) and half sphere (■, ■) samples, respectively.....	37

Figure 4.12 – Effect of geometry and chemical nature of printed samples on contact angles in water. Pyramidal (■) and half sphere (■) geometry, respectively. 38

Figure 4.13 – Effect of geometry and chemical nature of printed samples on contact angles in oil. Pyramidal (■) and half sphere (■) geometry, respectively..... 39

Figure 4.14 – Contact angle with correct factor measurement with water as the drop’s content in pyramidal (■) and half sphere (■) samples, respectively..... 40

Figure A1 – DSC of FOMM-60 filament before 3D printing and washing by heat flow and increase of temperature, with exothermic peaks and endothermic valleys. ...56

Figure A2 – DSC of FOMM-60 filament after 3D printing and before washing by heat flow and increase of temperature, with exothermic peaks and endothermic valleys. 57

LIST OF TABLES

Table 1.1– Drops diagram on solid surface with different degrees of spreadability and wettability and their corresponding contact angle values.	11
Table 3.1 – 3D printing parameters as the quality and geometry options.	22
Table 3.2 – Permeable membranes with different pattern and infill percentage.	23
Table 4.1 – Side view of HIPS 3D geometrical samples (pyramidal and half sphere) and HIPS permeable membrane samples with 50% and 25% triangular and hexagonal infill, respectively.	25
Table 4.2 – Side view of FOMM-60 3D geometrical samples (pyramidal and half sphere and FOMM [®] -60 permeable membrane samples with 50% and 25% triangular and hexagonal infill, respectively.	25
Table 4.3 – Water drop and surface Contact Angle Mean (CA _m), standard deviation (S), Contact Angle Mean (CA _m) with corrector factor and standard deviation (S) with corrector factor r, the corrector factor r and the roughness parameter (S _a and S _q).	41
Table 4.4- Oil drop and surface Contact Angle Mean (CA _m), standard deviation (S), and the roughness parameter (S _a and S _q).	41
Table 4.5 – Shape of water dropped on pyramidal and half sphere FOMM [®] -60 and HIPS samples.	42
Table 4.6– Shape of oil dropped on pyramidal and half sphere FOMM [®] -60 and HIPS samples.	42
Table 4.7– Shape of water dropped during the slippery test on pyramidal and half sphere FOMM [®] -60 and HIPS samples.	43
Table 4.8– Shape of oil dropped during the slippery test on pyramidal and half sphere FOMM [®] -60 and HIPS samples.	44
Table 4.9– Interaction between HIPS and FOMM [®] -60 samples with 50% of triangular and hexagonal infill and drops of water and oil at the moments: before the drop, the exact moment when the drop touches the material and a minute after the drops..	46

LIST OF SIMBOLS AND ACRONYMS/ ABBREVIATION

LIST OF SIMBOLS AND ACRONYMS/ ABBREVIATIONS

List of Symbols

- E – Modulus of Elasticity
 S_a – Arithmetical Mean Height
 S_q – Root Mean Square Height
 T_C – Crystallization Temperature
 T_g – Glass Transition Temperature
 T_m – Melting Temperature
 γ_{LV} – Liquid–Vapor Interfacial Free Energy
 γ_{SL} – Solid–Liquid Interfacial Energy
 γ_{SV} – Solid–Vapor Interfacial Free Energy
 W_0 – Initial Weight
 W_t – Final Weight
 θ – Contact Angle

Acronyms/Abbreviations

- 3D – Three Dimensional
AM – Additive Manufacturing
ANOVA – One-Way Analysis of Variance
CA – Contact Angle
CMC – Critical Micelle Concentration
DEM – Departamento de Engenharia Mecânica
DSC – Differential Scanning Calorimetry
FCTUC – Faculdade de Ciências e Tecnologia da Universidade de Coimbra
FDM – Fused Deposition Modeling

FTIR – Fourier Transform Infrared Spectroscopy

HIPS – High Impact Polystyrene

LQ – Low Quality

NQ – Normal Quality

PVA – Poly(vinyl alcohol)

PU – Polyurethane

TGA – Thermogravimetry Analysis

SEM – Scanning Electron Microscopy

INTRODUCTION

Mineral-based waste oils are not biodegradable and can cause serious environmental problems when not properly disposed. Approximately 42 million tons of oil are consumed annually worldwide and generate 22 million tons of used oil and only 40% of the lubricant is able to be reused. Usually, the process of retaining oil is impaired due to the presence of other compounds, such as water, which can compromise the oil reuse. Also, the use of oil as lubricant leads to its degradation and accumulation of contaminants. The procedures of oil changing, and cleaning can also lead to an oil/water waste.

Due to environmental issues, the oil removal from waste fluids is very valuable for the global ecosystems. Chemical processes are the most conventional approaches for oil/water separation, relying on the use of different surfactants in order to obtain stable emulsions. The use of these surfactants also contributes to the water pollution, demanding for further treatment steps in order to purify the residual wastewater. This process is usually complex and expensive and therefore not advantageous at laboratorial or industrial scale, since it requires specific equipment and procedures to achieve significant oil/water removal yields.

Physical oil/water separation procedures can be regarded as a greener, easier and cheaper alternative since it is a surfactant-free system and can also reduce costs with equipment, workers and time. These procedures are based on physical interactions between the mixture and specific substrates and relies on hydrophobic/hydrophilic interactions and other surface properties such as surface area, roughness and geometry.

Additive manufacturing technologies (AM), commonly known as 3D printing technologies, can be used to design complex and specific structures, constituted by mono or multimaterials, with potential application in oil/water separation by means of physical procedures.

In order to overcome the current oil/water separation methods limitations, the present work intends to study the possibility of using a 3D printing technique for the development of complex hierarchical structures and assess their effect on the wettability of polymeric material with different levels of hydrophobicity for separation of water/oil

dispersions. Thus, this study aims to explore the capacity of producing components, by 3D printing, with the ability to separate oil from water.

The first chapter presents a study based on literature survey on suspensions and separation process. Then, in the second chapter there is a summary of the project study. In the third, the project organization, the materials used and their study, the processes for obtaining the final object and tests for its evaluation are presented. In the fourth, the obtained results are presented and discussed. Finally, conclusions and proposals for future studies are presented.

1. STATE OF THE ART

1.1. Oil/water suspension, emulsion and the environmental problem

Oil/water suspensions or emulsions are common in industrial waste, such as food, cosmetics, chemicals, among others (1). Both fluids are commonly used and manufactured in pharmaceutical, cosmetic, chemical, petroleum, food and metal processing industries (2). Wastewater with oil content produced in those industries may result in environmental problems. Actually, oil/water solutions can damage the sewage network, compromising the functioning of the water treatment networks and even modify the environment's pH and diminish the gaseous rate exchange between water and the atmosphere. Moreover, under solar radiation influence, the oil temperature can reach 60 °C, compromising the maintenance of microscopic plant and animal species (3). Steel-mill, textile and chemical industries also produce oil/water suspension as waste. The engine lubrication and cleaning stage processes are the most problematic polluting areas regarding the industrial waste. Once in contact with water, the used oil and the detergent (surfactant) form a non-stable dispersion. Upon reaching rivers and seas this dispersion emerges through the water and lays on its surface, harming the environment (4).

Oil/water suspension is the combination of two liquids with little interaction with each other. Therefore, it is poorly stable and easily separated into distinct phases. However, a stabler and more homogenous dispersions can be obtained by the utilization of different variables such as temperature, agitation and presence of surfactants. The resulting solution is the so-called emulsion, where the type and chemical nature of a given surfactant plays a major role in determining the physicochemical stability of the emulsion. In turn, emulsions are the suspension of two immiscible liquid droplets mixed by force and stabilized by adding surfactants. Surfactants have amphipathic molecular structure and provide high solubility. They also display different functional groups with different affinity within the same molecule, making it possible to stabilize the immiscible solution (5; 6).

The correct way to dispose of this combination of liquids in order to avoid environmental damage is to separate the liquids and then recycle them individually. The most common separation treatments of these oil wastewater composed of oil/water suspension are

flocculation, distillation and demulsification followed by precipitation. The flocculation process is not effective and it must be combined with different methods, which increases its cost. The distillation and demulsification process are better choices regarding the process consistency. In the distillation process (Figure 1.1), the oil wastewater is heated until the water boils, as water boils before oil. The hot vapor phase goes to a condenser, where it is cooled and condensing in another compartment. The process goes on until the components are completely separated (7; 8). Since this is a long process, it is only for small volumes. Thus, in order to distillate a large flux ratio, fractionation columns should be used. Hitherto, it is a too expensive investment to treat a liquid that will be discarded (7).

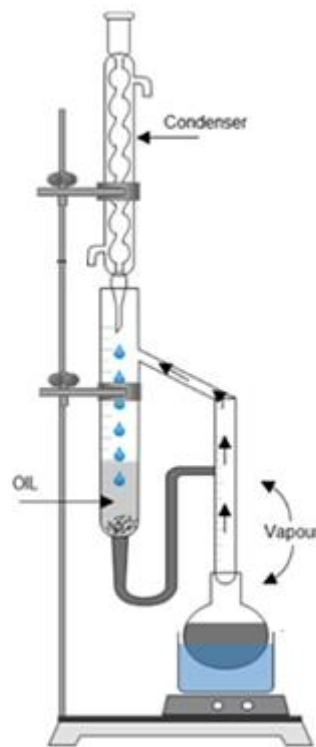


Figure 1.1 – Laboratory assembly liquid–liquid extraction (7).

Figure 1.2 shows a scheme of demulsification followed by precipitation process. The scheme represents a magnetic method of precipitation and the compound announced as MRGO is a magnetic demulsifier for oily wastewater from oil-in-water emulsions. The image shows a specific case, however in general the compound introduction breaks the interfacial

barrier between oil and water. This influence leads to the destabilization of the oil droplets, causing their coalescence. The droplets fuse and form a single layer on the top of the water (9).

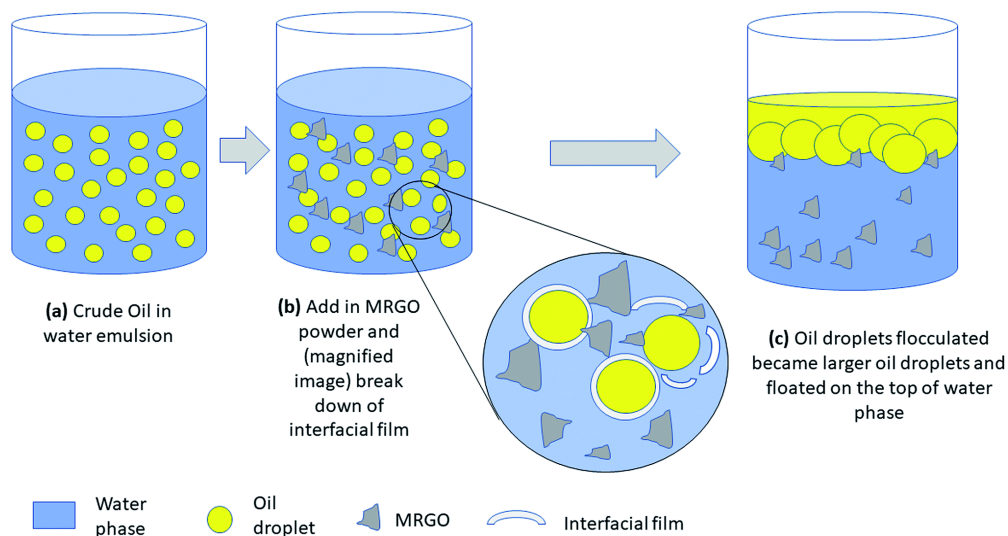


Figure 1.2 – Diagram illustrating the demulsification of oil-in-water emulsion process with a MRGO noncompound (9).

The demulsification followed by precipitation techniques use chemical agents or need to change the state of the solvent for aqueous separation, making the techniques expensive mostly due to the purchase of additives and high energy cost. The chemical method includes the addition of electrolytes (coagulants) and surface-active compounds (demulsifiers), leading to a decrease in drop charge and, as a result, phase separation due to drop coalescence. Adding a centrifugal force with heating to this process is common since it helps to improve liquid separation (10). An alternative is the mechanical separation process, which usually has low energy costs and smaller water consumption when compared with the chemical method. The microfiltration process with membranes is the mechanical separation process that stands out due to its productivity. In this system, the operational cost is only the equipment plus electric energy from the operation of the hydraulic pump. As heat exchangers are not necessary, problems related to thermal pollution and overload of the effluent system are avoided (11).

As the membrane/mesh separation process requires low maintenance and it is easy to operate, it is one of the simplest and more efficient process of separation. It works as a barrier, restricting some elements. Porosity and flow pressure of the suspension are important to the separation process, usually the greater the number of pores and the lower the flow the better are the results (9). Figure 1.3 exemplifies this type of mechanical process, which depends on the

type of mesh used and the gravitational force. When the mesh is hydrophobic, the oil is captured by the separator, whilst it is hydrophilic, the oil is repelled. Moreover, the mesh used depends on the component's density, since by gravity the flow is forced through the mesh, interacting with small substances and separating the mix (12).

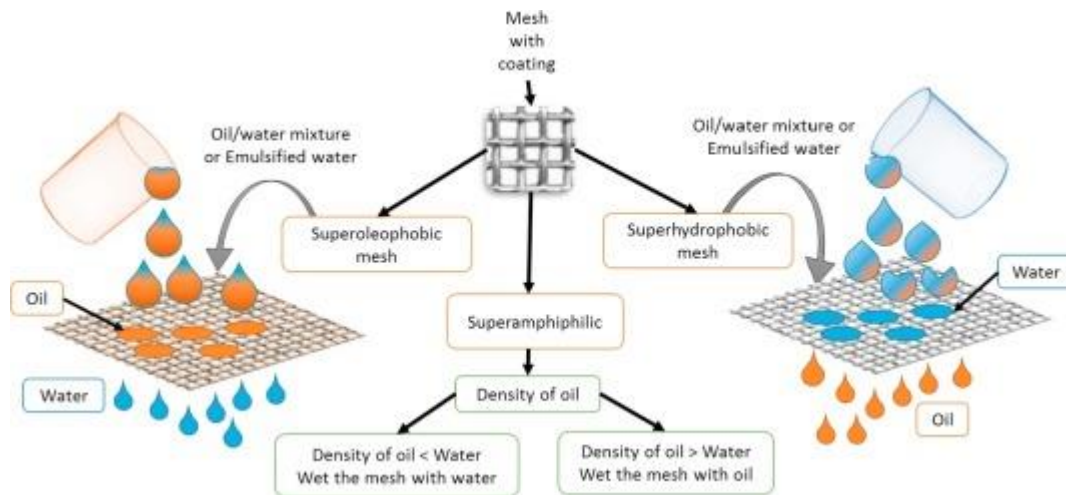


Figure 1.3 – Mechanical separation of oil and water by microfiltration process (12).

There are two kind of membranes that might be used in the membrane/mesh separation process: “oil-blocking” or “water-blocking” membranes, considering oil/water mixtures. The “oil-blocking” type membrane filtration techniques separate water from oil. This feature is provided by the membrane material superhydrophilic properties, which allow the water phase pass through the material. This system is considered better than the “water-blocking” process, which uses superhydrophobic and superoleophilic materials to separate oil from water, because this process avoids the surface fouling by oil, as the density of water is usually the higher one in the mixture. Another important characteristic is the presence of small pore sizes in the membrane, since it improves the contact between the material and the mixture, developing the separation process (13; 14).

1.2. Suspension / emulsion separation process

Emulsion can be divided into two categories: polar (hydrophilic) and non-polar (lipophilic) components, both related to what constitutes the mixture. One type of emulsion commonly used is water in oil emulsion, wherein there are water droplets dispersed in an oil phase. An oil in water emulsion are drops of oil in a water phase. In this last case, knowing the properties related to the stability of the oil drops is interesting to define its separation process (15).

Due to the small interaction between the oil drop and the water, the drops join with each other, forming larger drops until two distinct phases of oil and water are created. This effect is called coalescence and leads to phase separation (16). By agitation with a surfactant in concentration above its critical micelle concentration (CMC), new oil/water surfaces are shown. As the surfactant is directed towards the surfaces, the entire oil droplets get covered by the surfactant. The behavior described is schematized in Figure 1.4. It is also possible to notice the surfactant self-assembly property in the scheme, when the surfactant concentration is above the critical concentration if the interactions are only between surfactant and water (17).

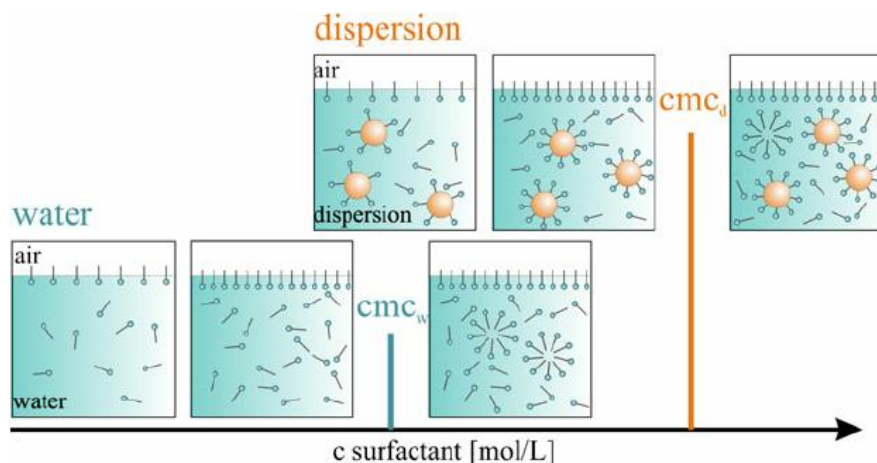


Figure 1.4 – Interaction between surfactants and molecules as the critical micelle formation concentration (CMC) is developed (17).

In case of the anionic surfactant, the oil droplets acquire negative surface charge. As all droplets have the same charge, they repel each other, avoiding contact between them. This scenario reduces the chances of coalescence. Nonionic surfactants have no real charges form droplets (do not have a double electrical layer), leading to a less stable emulsion compared with the anionic surfactant emulsions. In both cases though, if the oil droplets approach slowly,

they repel each other, not colliding and the layered emulsions of surfactants can still coalesce. However, when the approximation is stronger (i.e., high agitation), the droplet surfactant molecules can move around its surface, increasing the instability of the mixture. And, it is at this point that the action of demulsification has an effect (18).

Currently, chemical demulsification joined with air flotation is the most common technique used by industry for the treatment of oil emulsions. This process still involves the application of restricted chemicals followed by secondary purification, due to its contamination potential. The method involves the inhibition of the hydrophobic emulsifying agents by the reagent addition, allowing the water droplets to merge (19). Hence the chemicals destroy the emulsifying agent barrier, decreasing the repulsive effects of electrical double layers to allow oil droplets to coalesce. The air flotation method helps the droplets coalescence process because the air bubbles increase the collision between them, bringing the drops to the surface of the liquid (20). The results vary as the demulsifier is proper for the emulsion in treatment, the quality of the mix between chemical and emulsion and the adequate temperature. This chemical process declines its effectiveness with the presence of surfactants in the mixing, because they coat the surface of oil droplets, increase the repulsive forces against the components and it gets more complicated to break the emulsion. Other methods are combined with chemical demulsification to break emulsion, as centrifuging or heating (21).

Besides the method described above, demulsification by mechanical means do not entails the oil droplets disruption, but it leads to an interaction with a hydrophobic material, capturing the oil compound. The membrane mechanical separation process has no complexity equipment or process, once the fluid flows by gravity through membrane network pores (mesh) and depends on the membrane material. Therefore, the interaction between the membrane and one of the fluid components must be extremely good (22). To improve this interaction, besides the material properties, the surface's topography must be elaborated with different levels. Yet, if the selected material's mesh is superhydrophobic, unlike the hydrophobic mesh materials, a common problem seen is the mesh's pores obstruction due to the adhered oil and cleaning difficulty (23). In recent works regarding emulsion filtration, it has been noticed that the emulsion filtration success depends on the rate between the droplet and the pore diameter. When this rate value is higher than one, the droplet deforms and shatters, weakening the filtration process (2).

There is also another type of separation process that involves wettability and materials with specific properties of chemical composition and surface topography, such as geometric structure. This process is physical and depends on the contact between the suspension and the material. The most valuable materials to the separation process are the ones with high wetting rate, complex surface morphology, good spheric liquid droplet formation and slide on the hierarchically structure. This kind of technique is recent and under development. Overall, it would be a simple separation way as it only involves a multi-structured material. However, the production of this material is complex since it depends on many variables (24).

1.3. Suspension / emulsion separation technology by physical processes

According to the literature survey, superhydrophobic materials provide effectively oil/water separation, once the avoidance of water and affinity to organic liquids leads to the absorbance of oil into the cavities of the material (25). It is vital for the separation process to control the liquid adhesion on the surface, since the dynamic action between liquid and surface is determined by the adhesion. This property is controlled by the surface chemistry and roughness. Another important feature of the procedure is to select the right material (surface) and conditions to improve the separation process. Thus, the hydrophobicity of a given material is increased by the surface properties, depending on the surface tension and contact rate between the water droplet and the rough surface (23; 24). A surface with high energy presents a low contact angle (hydrophilic surface) in water, whilst a low-energy surface provides a high contact angle (hydrophobic surface). The liquid molecules search for a low energy position to fill, with forces (attractive and repulsive) acting in all directions. When contact angle is too elevated, the adhesion between liquid and solid does not exist, since the liquid does not show wettability, which promotes hydrophobicity (26; 27).

In line with these studies, the greater the roughness complexion and geometry the wider the interaction. If the material also has hydrophobic properties, besides the expelling of the drop of water, it will have a high oil absorption content. Furthermore, the surface roughness influences on slipping behavior of the water droplet. The increasing of the surface roughness leads to a completely roll off of the water drop. To evaluate a rough surface using the Wenzel model as shown in the Equation (1.1), it is possible to justify the influence of roughness on the solid surface wettability. The contact angle is studied by the spread of a drop of water on a

rough surface. Since r_w is the ratio between the real and projected rough surface area, an energy balance is performed as is shown in Equation (1.1) (28; 29).

$$\Delta G = \Delta A_R (\gamma_{SL} - \gamma_{SV}) + \Delta A_P \gamma_{LV} \cos \theta^* \quad (1.1)$$

where ΔA_R is the rough area covered by liquid, ΔA_P is the projected area and θ^* the contact angle between liquid and the rough surface. By minimizing the surface energy, the equilibrium situation is obtained:





$$\Delta \cos \theta^* = r_w \cos \theta \quad (1.2)$$

where θ is the contact angle between the liquid and a solid smooth surface.

The mathematical model proves that the roughness effect increases the hydrophobicity of hydrophobic surfaces (if $\theta > 90^\circ$ e $\theta^* > \theta$) (29).

Wenzel's equation assumes that the drop of liquid is in full contact with the rough surface and that the surface is chemically non-uniform. Another equation called Cassie-Baxter is used when a material exhibits a rough, porous surface. It assumes that the drop cannot completely reach the rough surface because of air pockets that are formed between the liquid and the material area. This feature causes the Cassie-Baxter state to reveal a smaller wet area and a larger contact angle value than Wenzel's. Wenzel is the most used equation and ensures that a greater number of materials and surfaces are represented (30). Table 1.1 shows the rate between hydrophilicity and contact angle, which varies between 0 and 180°, as well as the respective formats referring to the wettability and spreading of the drop. The first composition of Table 1.1 displays a situation where liquid wets the surface completely, the so-called hydrophilic surface. In the last one, it shows the complete opposite where the drop is a perfect sphere and thus super hydrophobic (31).

Table 1.1– Drops diagram on solid surface with different degrees of spreadability and wettability and their corresponding contact angle values.

Property	Super hydrophilic	Hydrophilic	Hydrophobic	Super hydrophobic
Drop diagram				
Contact angle	$\theta < 10^\circ$	$\theta < 90^\circ$	$\theta > 90^\circ$	$\theta > 150^\circ$

1.4. Suspension / emulsion separation by hierarchical roughness and surface properties

Some plants' leaves are known to expel water droplets (exhibit superhydrophobic surfaces) due to the presence of a hierarchical roughness (on the metric scale) on its surface, presenting protrusions and protuberances (32). This morphology confines air at the interface between the liquid and solid surface, attributing to it a hydrophobic effect, which is called the Lotus Effect. An example of the mentioned topography is shown in Figure 1.5. Studies have also shown that the insertion of micropatterns by lithography with the shape of polymers' towers affects the values of contact angles and droplet size. This fact shows that this type of additional topographic formation stabilizes air bags and intensifies the water droplets rejection (31).

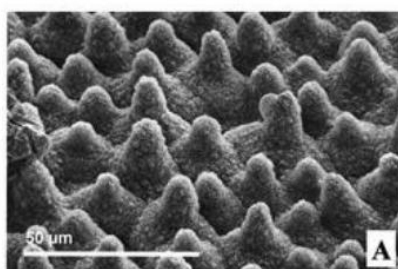


Figure 1.5 – SEM images of a hydrophobic plant (A) *Nelumbo nucifera* (lotus flower) (31).

The scientific community gets inspired by naturally hydrophobic surfaces with different geometries found in nature to replicate, on a laboratorial scale, material with similar surface properties. Recent works by Yang et al. (24) shows the "Salvinia effect" (Figure 1.6(a)), which is a behavior displayed by a leaf with a geometric shape that retains long-term air and also fix water drops. The study shows the printing of a leaf inspired object that presents a hierarchical architecture surface composed of eggbeater shaped hair strands coated with nanoscopic wax crystals and hydrophilic parts along its cells. These eggbeater shaped structures could be synthetically formed in smaller sizes than the original leaves ones by lithography. If the contact angle is smaller than 150° it is not a super hydrophobic structure. Thus, to increase the contact angle, coating the surface with carbon nanotube could be a good solution. The "lotus effect" shows a large contact angle ($CA \approx 161^\circ$) and a low sliding angle (2°) on the surface. However, the "petal effect" (Figure 1.6(b)) of the eggbeater shaped surface besides showing super-hydrophobicity ($CA \approx 152^\circ$), also displays a strong adhesion that retain water droplets (24).

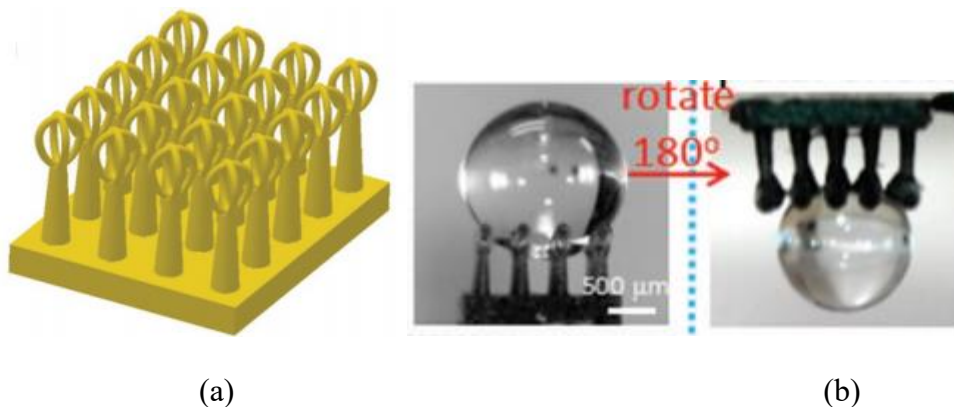


Figure 1.6 – “Salvinia effect “(a) eggbeater shaped surface morphology (b) “petal effect” of the eggbeater shaped topography (24).

For an oil/water separation system it is important to build a hierarchical structure with micro/nanoscale spaces to improve oil uptake and water repellency, in other words, the material's porosity must be increased. The size of these spaces may vary between 1 to $5 \mu\text{m}$ and these structures must be hydrophobic materials with free energy surface (33). Another approach

to improve the repellency of water droplets is to control the material's geometry, adding free spaces/pores to the surface (i.e., cavities, mesh). The methodology that relates the contact angle between water drop and the surface is shown in Equation (1.3).

$$\cos\theta^* = \varphi_s \cos\theta + (1 - \varphi_s)(-1) \quad (1.3)$$

, where θ corresponds to the contact angle of the solid material without structures / permeable membrane surface. φ_s is the solid fraction of the surface area and $1-\varphi_s$ is the area fraction of the liquid/air interface. The three patterns of microstructures that suit the better to retain air in their cavities are shown in Figure 1.7, with a top view of the cavities. Morphologies containing towers or large protrusions tend to let water penetrate through capillarity, reducing the hydrophobic property of the material (33; 34).

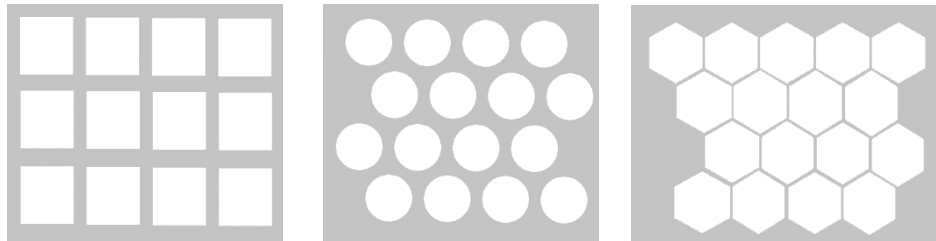


Figure 1.7 – Top view of the patterns chosen for the microstructures. The white regions correspond to a high plane and the gray regions to a low plane. Where (a) square, (b) round e (c) hexagon.

Even though the hierarchical roughness affects the contact angle and the surface wettability, it has not yet been completely predicted how it contributes to the development of these features (32).

2. WORK PROJECT

2.1. Motivation

To study the surfaces roughness and geometry effect on the water/oil systems separation, the 3D printing (Additive manufacturing – AM) technique will be used to produce highly complex structures with the desired properties and designs. The aim is to produce a 3D printed device and evaluate its wettability, by analyzing the interaction of oil and water with the surface of a hydrophobic polymeric material with complex geometry and hierarchical surface roughness.

2.2. Material Processing - 3D Printing

3D printing is an additive manufacturing technique that creates a 3D model from a computational model and it will be the main process technique. There are seven varieties of 3D printing technologies: Binder Jetting, Directed Energy Deposition, Materials Extrusion, Materials Jetting, Powder Bed Fusion, Sheet Lamination and Vat Photopolymerization (35). Selective Laser Melting (SLM) is the most common 3D technique used and it is a promising method in the PBF category. SLM uses the laser to fully melt the metal powder to form a homogeneous part (36).

The main advantage of 3D printing is the creation of a unique item, allowing the construction of a material with a complex and specific porosity and topography, which will help the polymer wettability study and the understanding of which factors maximize or minimize the repellency of drops of water. The method designs structures for 3D printing technology to obtain detailed objects using Fused Filament Fabrication (FFF) (37). This technology prints by layers, extruding a plastic filament. The 3D printing process starts with a 3D model made in a modeling program. In this process, a thermoplastic material filament is pushed into an extruder. The temperature of the extruder is above glass transition temperature. There is a nozzle at the end of the equipment and the molten filament is extruded through it, driven by rollers. It is then

placed on top of a flat printing bed or previously printed layer. The printer then builds a physical object from the 3D model, laying down layers of material (Figure 2.1). Object production is fast and cost-effective. The main problem of this type of 3D printing is the created object surface finish, which usually is rough and with poor strength (38). The mechanical strength in in-plane directions of the FFF produced part that is reduced in this type of process and can be corrected by printing the objects under vacuum or a possible thermal treatment after printing reduces the part porosity and roughness. However, these are methods that turn the process very expensive (39).

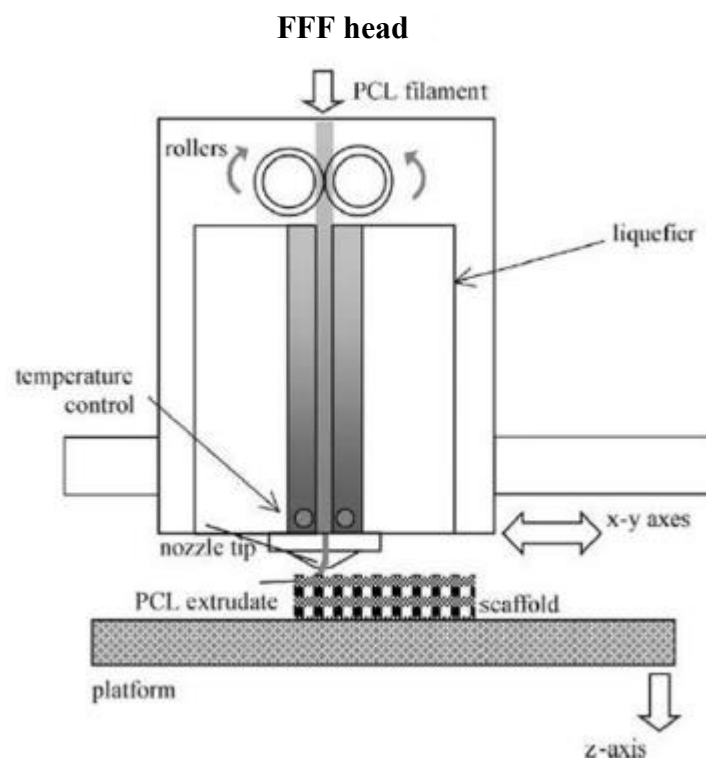


Figure 2.1 - Schematic of FFF adapted from (40).

As an example, the Figure shows how the molten filament flows inside and through a nozzle. In Figure 2.2 (a), the molten filament frictionates with the nozzle wall, stretching the polymer chain. The nozzle inner diameter decreases, which increases the flow velocity and stretches more the filament (Figure 2.2 (b)). The molten polymer flow goes from vertical direction to be horizontally placed, while a compression and tension from the upper and lower sides of the polymer happens, shown in Figure 2.2 (c;d) (39).

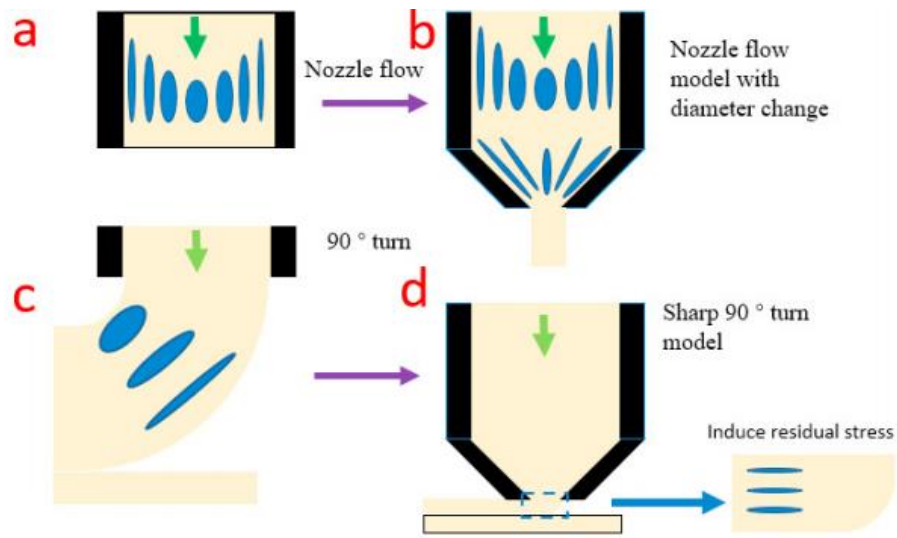


Figure 2.2 - Schematic diagram of (a) (b) nozzle flow and (c) (d) horizontal turn (39).

Some studies have shown the printing of hierarchical structures with small air pockets, formed by uneven surfaces. A decrease of sliding angle and adhesive force are shown by these studies' objects, which results in superhydrophobic surfaces. This kind of surface may be obtained by increasing the roughness and porosity during the printing method (41).

2.3. Materials

High Impact Polystyrene (HIPS) and FOMM[®]-60 were the two materials chosen to be used on this study. The selection was made by the materials interaction with water and oil, separately; HIPS has a hydrophobic character and FOMM[®]-60 a hydrophilic character. The HIPS material is mainly assembled by polystyrene, which shows as main characteristics an impact-resistance and an easily thermoformability. The easily thermoformability feature is important in this study because of the high temperature of the step of extrusion in the 3-D possessing used throughout the essay (42). The HIPS standard distilled water wettability measurements demonstrate that the material by itself has a contact angle value of $88.2^{\circ} \pm 1.5^{\circ}$ (43). The chemical structure of HIPS is shown in Figure 2.3.

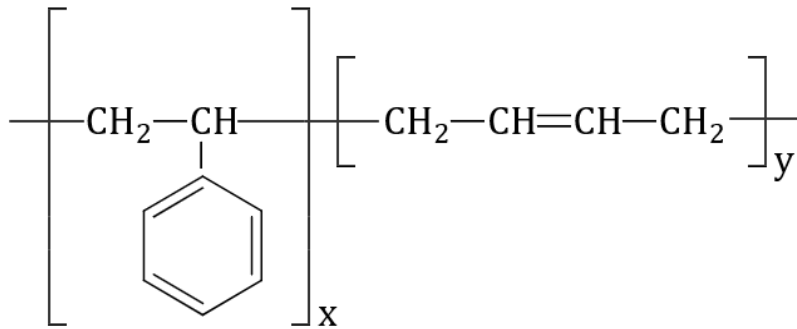


Figure 2.3 – High impact polystyrene chemical structure (44).

In turn, the FOMM[®]-60 material is composed by a water soluble polymer, poly (vinyl alcohol) (PVA) and polyurethane (PU). PVA is water-soluble, hydrophilic but with significant tensile strength and hardness (45). PU polymer is soft and hydrophobic and shows excellent elastomeric properties and high durability (46).

After the material has been extruded by the 3-D printer and become a sample with a particular shape, it was washed and dried in an oven for 5 h at 50 °C, which is the major temperature used to avoid shape alteration. This process is important to make the FOMM-60 samples PVA free and as result a material with flexible and microporous features (47). This is a relatively new material and there are no wettability measurements data available in the literature, so far. The PVA functional structure is shown in Figure 2.4.

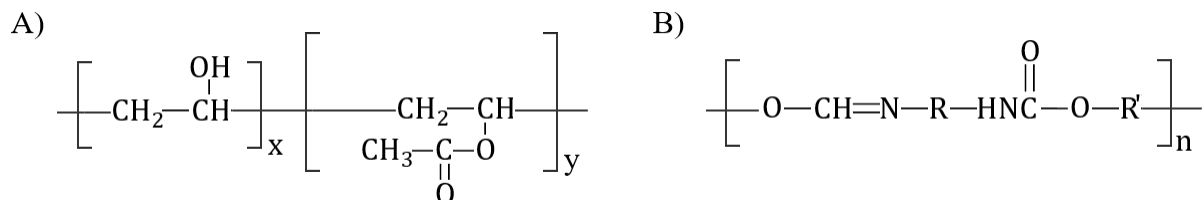


Figure 2.4 – Chemistry of the unit structures of (A) PVA (48) and (B) TPU (49).

3. MATERIALS AND METHODS

3.1. Materials

High Impact Polystyrene (HIPS, melting temperature: 150 - 180 °C) was purchased from DoWire®, Seixal, Portugal. FOMM®-60 was obtained from filament2print company (Barcelona, Spain). All filaments are 1.75 mm in diameter.

3.2. 3D Printing

3D-printing techniques allow the printing of complex structures, it was used FFF technique. FFF is a common 3D processing technique and provides with low cost high application range. To start the 3D printing process, a 3D model is made in Computer Aided Design (CAD). The stl file is processed in a slicing program where all the printing parameters are selected. The obtained gcode file is then transferred to the printer, which will print the object precisely based on that data. In this technique stacks fused filaments in multilayers and creates rough surfaces, providing different size and shape of the designed structures and the printing quality settled to print the samples varies between normal and draft quality. In this study, samples of two distinct polymers, FOMM®-60 and HIPS, were printed. Also, two 3D geometries were analyzed and compared, pyramidal and half sphere, both were printed in the two qualities described. In addition, bases with different infills were also studied. The infill of the bases ranged between 50 and 25% with triangular and hexagonal geometries. FFF printing process shows different results from the 3D printing. The main parameters that create variations are extruder temperature, bed temperature and printing speed, which have a high effect on the adhesion force of the manufactured material (50). To build the HIPS and FOMM®-60 samples the extruder temperature was 240 and 230 °C, the bed temperature was 110 and 70 °C and the printing speed was 40 and 25 mm/s, respectively.

3.3. Characterization Techniques

3.3.1. Fourier Transform Infrared Spectroscopy (FTIR)

The FTIR is useful to identify functional groups by chemical bonds. The equipment records the molecule vibration when exposed with specific wavelengths of light. The data is plotted by the vibration intensity (% absorbance) and frequency of light (cm^{-1}), producing a FTIR spectrum. Different vibration intensity and frequency correspond to a unique chemical functional group, making it possible to identify the components of a sample (51; 52).

The infrared spectra of the filaments were obtained from the FTNIR/MIR spectrometer (PerkinElmer, Frontier model) with Attenuated Total Reflectance (ATR), an FR-DTGS detector and a beam splitter. Each IR spectrum was obtained over the range of 500 - 4000 cm^{-1} with a resolution of 4 cm^{-1} and was analyzed using the SPECTRUM 10 STD software.

3.3.2. Thermogravimetry Analysis (TGA)

To better understand the material resulting from the 3D printing process, the TGA method was interesting to study the thermal degradation limit. Then, TGA is a simple technique to determine the material thermal stability (51).

TA instruments TGA Q500 V20.13 equipment was used in the analysis of the thermal stability of the filaments. The heating rate used was 10 $^{\circ}\text{C}/\text{min}$, as a constant nitrogen flow and temperature range was 25 - 600 $^{\circ}\text{C}$. The results were studied using the TA Instruments Universal Analysis software.

3.3.3. Differential Scanning Calorimetry (DSC)

Differential Scanning Calorimetry (DSC) is a technique used to measure the energy transferred to or from a sample during a thermal change, such as glass transition temperature (T_g), crystallization temperature (T_c) and melting temperature (T_m). The method analyses the sample energy consumption or releasing as the temperature changes, during a controlled temperature program. The energy is measured as heat and these transitions are later identified as the heat flux rate profile, which allows the identification of polymeric materials thermal events (53).

TA instruments DSC Q100 V9.9 equipment was used for the sample's thermal characterization. The heating rate used was 10 °C/min, with a constant nitrogen flow. The filaments temperature range was -100 to 300 °C for HIPS, -100 to 200 °C for FOMM-60. The maximum temperature was chosen based on the TGA characterization. Thus, the maximum temperature used in the DSC method could not be the material degradation temperature. The results were analyzed using the TA Instruments Universal Analysis software.

3.3.4. Scanning electron microscopy (SEM)

Scanning electron microscopy (SEM) are used to study the sample morphology. The technique scans the samples surface with a low energy focused electron beam and the detection of the backscattered or the secondary electrons emitted is used to create an image in the nanometer range (54; 55).

The MERLIN™ FE-SEM was the instrument used to obtain the images of the samples surface. The apparatus displays a double condenser system, which made it possible to achieve surface high resolution images of 2 μm. The beam currents used was of 93 pA and no coating process was made for the evaluation of the surface. Also, the method was carried out with the sample already printed in two different moments, with the sample dried and the other one when they are already washed.

3.3.5. Water-swelling test

The execution of the water-swelling tests consists in immersing the sample on a water solution. The method helps to study the amount of water the sample may soak throughout time, leading to the determination of the swelling rate. Moreover, after the soaking process, it is possible to evaluate if the samples have lost any of its compounds.

The technique starts with the sample's initial weight record (W_0), following with the immersion of the sample in water. The sample was removed after some time immersed, superficially dried by a tissue paper and reweighed (W_t). The water-swelling ratio was calculated by the Equation (3.1) (56). The assays were performed in duplicate over 72 h.

$$S_W = \frac{W_t - W_o}{W_o} * 100\% \quad (3.1)$$

where S_w is the water-swelling ratio of the sample, W_0 is the initial sample's weight in grams and W_t is the sample's weight in grams after its immersion on a solution.

3.3.6. Contact angle

The wetting characterization method was done by an optical method, measuring the angle between a droplet and the surface, from which contact angle can be calculated. Although, the Wenzel model describes that there might exist a connection between surface roughness and its wettability, as the roughness may affects the contact angle measurement, the contact angles are also corrected with the factor r (26).

The first method to obtain the contact angle was a manual one. A 20 μl volume drop was dripped onto each one of the geometric surfaces with a pipette. In this first technique the contact angles were not corrected by the roughness factor and the pictures were made after the drop sits for 30 s. After this, an essay was performed using 10 μl volume drop that was dripped onto each one of the studied samples by the precision equipment (Optical Tensiometer – Teta topography) to obtain the contact angle between the surface and the drop. At this point, the contact angle was corrected and both values, with or without the roughness correction, were evaluated.

In both methods all samples' surfaces were horizontally aligned in order to evaluate the contact angles by the software OneAttension ver. 4.0.6

3.3.7. Slippery drop test (oil and water)

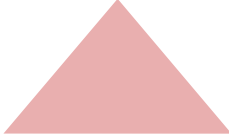


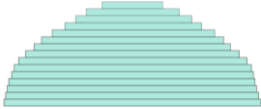
To achieve more factors related to wettability and adhesive characteristics and different printing mold resolutions, two types of water droplet slip test were performed. The first test consists in dropping an oil droplet repeatedly onto the surfaces with a syringe. The same procedure was performed for water droplets. Afterwards, the second type test was performed. This study drops volume was 5 μl of both water and oil and they were dripped onto the samples by the precision equipment (Attension Theta with 3D Topography Module), also at separate time. Also, their movement along the surfaces was recorded for 30s by the equipment. The samples were aligned vertically, with its base on the support. (29).

3.4. Printing pattern

In this study, four different rough pyramidal and half sphere samples were build using a software. The roughness was low when the printing option was Normal 0,2 (NQ) or high if Draft 0,4 (DQ). Also, four porous permeable membrane structures, bases, were also designed and the infill shape was either hexagonal or triangular. The designs were uploaded to 3-D printer and the samples were build layer by layer and are shown in Tables 3.1 and 3.2.

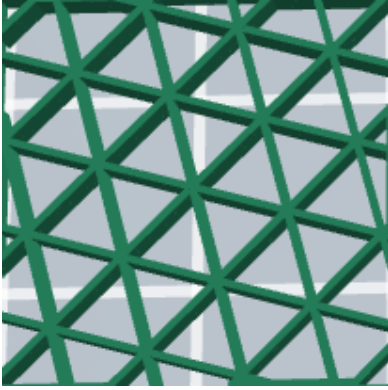
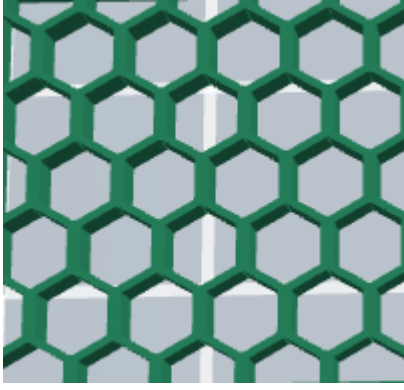
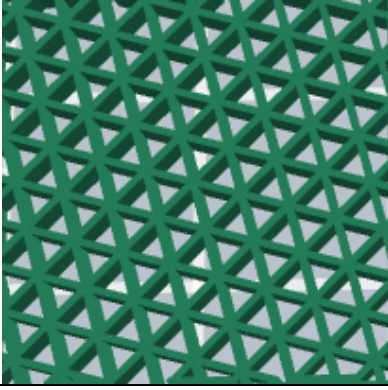
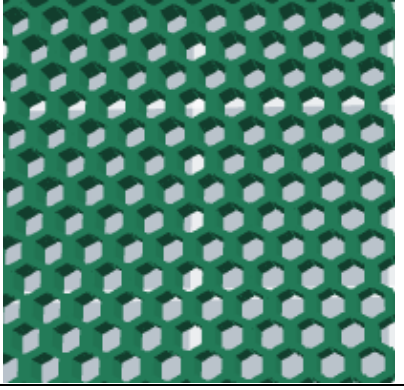
The printer extrusion temperature, bed temperature and printing speed for the FOMM[®]-60 samples were 230 °C, 70 °C and 25 mm/s, respectively. Yet, for the HIPS ones the printer extrusion temperature, bed temperature and printing speed values were 240 °C, 110 °C and 40 mm/s. The layer thickness adopted in all cases was 0.4 mm.

Table 3.1 – 3D printing parameters as the quality and geometry options.

Printing quality	Pyramidal sample	Spherical sample
NQ		
DQ		

Other important feature of the printed permeable membranes is the pores sizes. The permeable membranes samples differentiate not only on the infill geometry, but also on the infill percentage.

Table 3.2 – Permeable membranes with different pattern and infill percentage.

Infill percentage	Triangular pattern	Hexagonal pattern
25%	 A 3D perspective view of a green, triangular-patterned permeable membrane. The structure consists of interconnected green beams forming a grid of triangles. The infill percentage is 25%, meaning the solid material occupies one-quarter of the total volume.	 A 3D perspective view of a green, hexagonal-patterned permeable membrane. The structure consists of interconnected green beams forming a grid of hexagons. The infill percentage is 25%, meaning the solid material occupies one-quarter of the total volume.
50%	 A 3D perspective view of a green, triangular-patterned permeable membrane. The structure consists of interconnected green beams forming a grid of triangles. The infill percentage is 50%, meaning the solid material occupies half of the total volume.	 A 3D perspective view of a green, hexagonal-patterned permeable membrane. The structure consists of interconnected green beams forming a grid of hexagons. The infill percentage is 50%, meaning the solid material occupies half of the total volume.

4. RESULTS AND DISCUSSION

4.1. 3D samples

The geometric shaped samples were built as pyramidal and half sphere, and they differed themselves in terms of material and roughness. The permeable membrane samples were also made by distinct materials, but with different infill shapes and percentage (Tables 4.1 and 4.2). The materials used were HIPS and FOMM[®]-60, the roughness DQ and NQ and the infill shapes were triangular and hexagonal with 50% and 25% of empty spaces. These different types of samples were chosen to evaluate how the material and infill geometry affect the interaction between oil and water drops and both materials.

The printing process allowed the production of different patterns with different materials, shapes and roughness. Different roughness values were obtained varying the height of the printing layers. The permeable membrane samples infill variation allowed the samples to have different porosities. Thus, the roughness was another feature that influences in the materials' interaction with oil and water drops.

Afterward, the FOMM[®]-60 samples were submitted to a soaking process. The samples stayed in water for 30 min to 1 h and were agitated by an ultrasound equipment to remove the PVA present in the material. A change of the samples' color and texture was noticed at the end of the process, since they got lighter and softer. It is essential that the samples are completely dry before further analysis, once the water may interfere in the results. Thus, the FOMM[®]-60 samples were completely dried off in an oven, with a temperature of 50 °C for 5 h. This process was essential as the PVA could compromise the interaction results of the FOMM[®]-60 samples.

Table 4.1 – Side view of HIPS 3D geometrical samples (pyramidal and half sphere) and HIPS permeable membrane samples with 50% and 25% triangular and hexagonal infill, respectively.

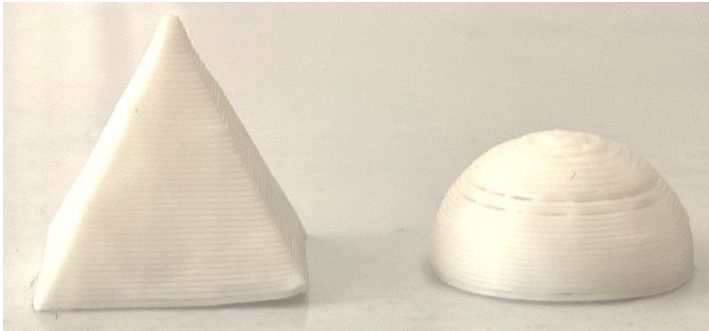
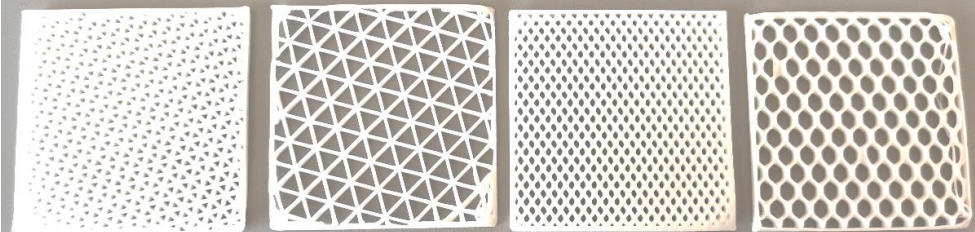
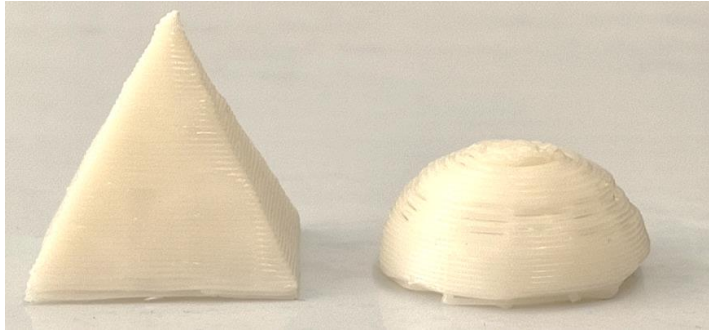
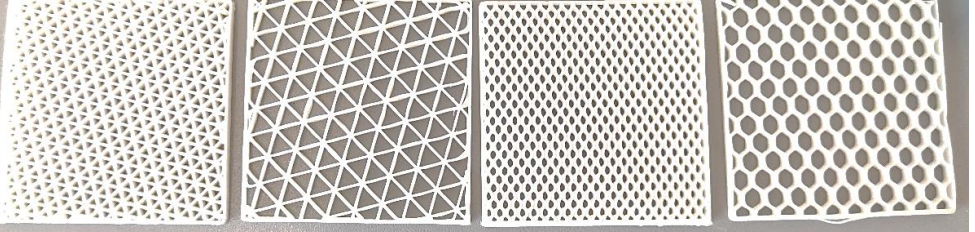
Material	HIPS
Geometric Samples	
Flat Samples	

Table 4.2 – Side view of FOMM-60 3D geometrical samples (pyramidal and half sphere and FOMM®-60 permeable membrane samples with 50% and 25% triangular and hexagonal infill, respectively.

Material	FOMM®-60
Geometric Samples	
Flat Samples	

4.2. Chemical characterization

4.2.1. FTIR

FTIR analysis was performed to identify the chemical groups existing in the filaments used in this work. This experiment allowed the identification of the characteristic bands of each 3D printed structures. Figures 4.1 and 4.2 represent the infrared spectrum of both HIPS and FOMM[®]-60 samples in a range of 500 – 4000 cm⁻¹, respectively.

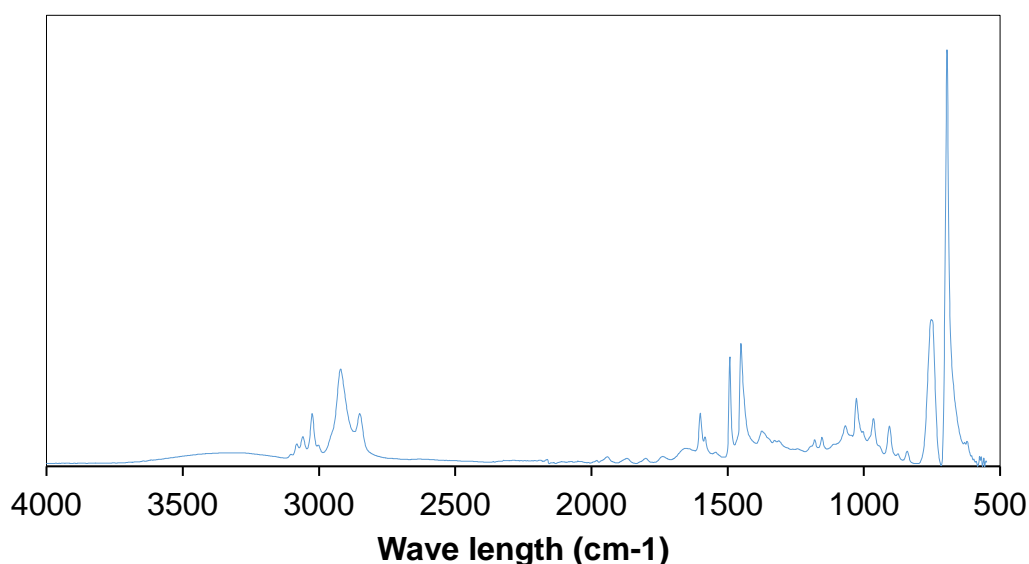


Figure 4.1 – FTIR spectrum of HIPS filaments.

Figure 5.1 shows the characteristic chemical bands of HIPS located between the 1400 and 1600 cm⁻¹ and 2500 and 3500 cm⁻¹. The first band positions are attributed to the deformation vibrational modes of the butadiene and the aromatic ring's C=C double bonds and the second band positions to the methyl single bond, which are the characteristic bands present in the HIPS polymer chain (57).

The FOMM[®]-60 does not have a complete analysis of its chemical groups in previous studies. Thus, the spectra of some possible polymers were used for comparison. Figure 4.2 shows FOMM[®]-60 FTIR spectra before and after washing procedures (in order to remove its PVA content). FTIR analysis was performed not only to analyze the functional

groups of the FOMM[®]-60 in the samples, but also to confirm the removal of PVA after washing procedures.

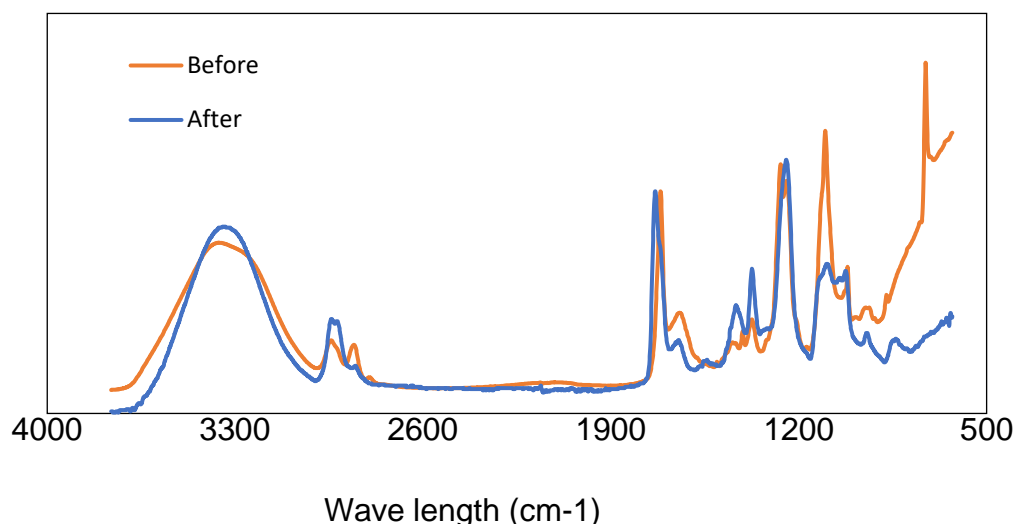


Figure 4.2 – FTIR spectrum of FOMM[®]-60 filaments before and after the soaking process, normalized by the most intense peak of each spectrum, respectively 1734 cm⁻¹ and 0,08 cm⁻¹.

Before the soaking process, the PVA characteristic chemical bands of O-H and C=O were verified around 2900 and 3300 cm⁻¹ and 1700 cm⁻¹, respectively. After the soaking process, there were peaks in the same range, but with less intensity, indicating that the washing procedure removed most of the PVA of the sample. The remain peaks of O-H in the spectrum may indicate the presence of water, once the drying process may not remove the water completely on the sample's chain after the soaking process. Also, after this process, the presence of other characteristic chemical bands may be suggested, such as NH groups (range of 3330 cm⁻¹), -C=O of ester groups (1700 cm⁻¹), amide II and amide III (1200 and 1500 cm⁻¹), C-O-C- (1150 cm⁻¹) and -CN- (1100 cm⁻¹) (58; 59). The evaluation of the data showed that the FOMM[®]-60 samples have unidentified chemical groups composition, due to the complexity of the material. However, the analyses indicate that the material is a polyurethane-based material, but the analysis cannot be confirmed with this only test.

The chemical components identification by bands is important to evaluate the interaction between the materials and the oil and water droplets, as this interaction may depend on the affinity among the compound's chemical chains in contact. Hence, studies showed that compounds that display polar groups tend to be hydrophobic, while those that

present nonpolar groups tend to be hydrophilic (60). Both polystyrene (PE) and PU are hydrophobic (42; 46), but the presence of other components in their chemical chain can make them less or more hydrophilic. The PE chain is mainly made of hydrocarbon bonds, which is very non-polar. The FOMM[®]-60 material exhibits PU, which has some polar and non-polar groups along its chemical chain, in addition to bonds of unidentified compounds. Some of these compounds display esters and amines groups, which are polar and could make the FOMM material more hydrophilic (61).

4.2.2. Water swelling test

In order to study the behavior of the substrates in water, a water swelling capacity test was carried out for the HIPS and FOMM[®]-60 printed samples. Moreover, the test was interesting to evaluate the amount of PVA in the FOMM[®]-60 material composition.

The water swelling capacity test was performed during 168 h for the FOMM[®]-60 material and 72 h for the HIPS material. The percentage of weight and loss in water of the FOMM[®]-60 and HIPS filaments are shown in Figure 4.3. The FOMM[®]-60 material underwent a fast and high mass gain, followed by a weigh stabilization, while the HIPS materials showed a small initial mass increase, which gradually descended and got stabilized. Both weight gains happened because of the uptake of water from the environment. The FOMM[®]-60 material has about nine times greater a swelling capacity than the HIPS material. This reveals a hydrophilic character of the material, which confirms previous analysis.

The loss of mass recorded around 30 h of FOMM[®]-60 material testing was probably due to the removal of the PVA integrated in the material by dissolution mechanism. This process is observed due to the high diffusion rate of the hydrophilic PVA into water and promotes pores formation in the material matrix due to the material exit. The subsequent retention of water by the material indicates the presence of hydrophilic chemical groups, besides the PVA, giving the material a “sponge” characteristic. This feature implies that the FOMM[®]-60 material will probably interact better with drops of water than oil ones. So, during a separation process, the material will tend to draw water out of the suspension, not oil.

The swelling measurements also allowed to quantify the amount of PVA in the FOMM[®]-60 material. The determination was made by the comparison of weights and the samples were weighted before the process started ($W_0 = 0,90\text{g}$). After the sample has been soaked in water, it was dried in an oven at $50\text{ }^\circ\text{C}$ for 5 h and reweighted ($W_f = 0,77\text{g}$). The PVA content in the material calculated was 15% and the swelling ratio was $79,2\% \pm 0,01\%$. The small mass increase observed in the HIPS water swelling test showed that the samples have some hydrophilic chemical groups, which due to their chemical affinity with water, form a molecular bond between the substrates by diffusion process. Besides, when comparing the HIPS with the FOMM[®]-60 samples water swelling capacity, the HIPS materials have a more hydrophobic behavior, whereas the FOMM[®]-60 samples have a hydrophilic one. This FOMM[®]-60 behavior may be displayed due to the polar chemical chains observed during the FTIR test.

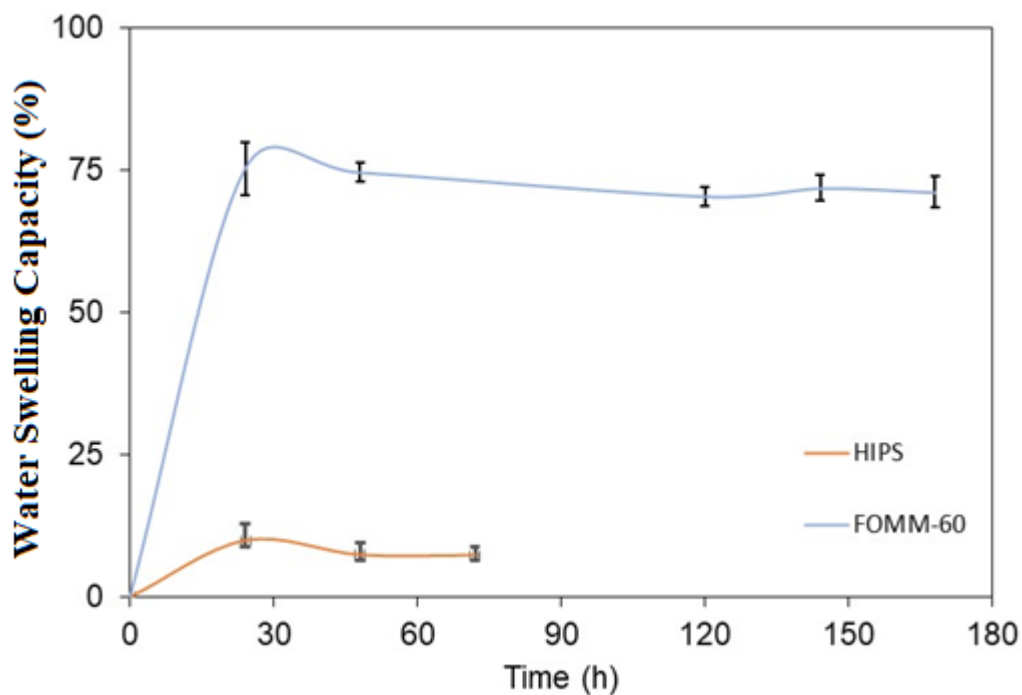


Figure 4.3 – The water uptake capacity of the FOMM[®]-60 and HIPS printed samples.

4.3. Thermal analysis

The thermal stability of the materials used in this study was evaluated by TGA technic. The thermogravimetric (TGA) and its derivatives (DTA) profiles are shown in Figures 4.4 and 4.5.

The TGA analysis identifies in how many stages the thermal decomposition of the material occurs when performed with the DTG graph analysis. A previous study showed that the HIPS thermal deterioration takes effect in a single stage between 350 and 500 °C. The degradation of HIPS in the present analysis follows the pattern described, with the same single stage of degradation between 370 and 485°C. The DTG profile shows that the reaction occurs in a single step and within a narrow temperature range close to 440°C (62).

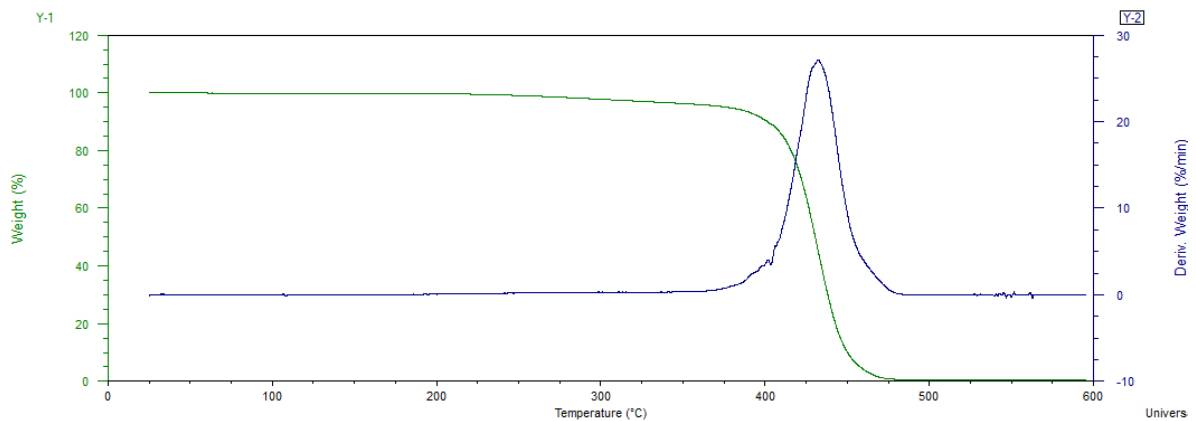


Figure 4.4 – Thermogravimetric and TGA derivative (DTG) profiles of HIPS.

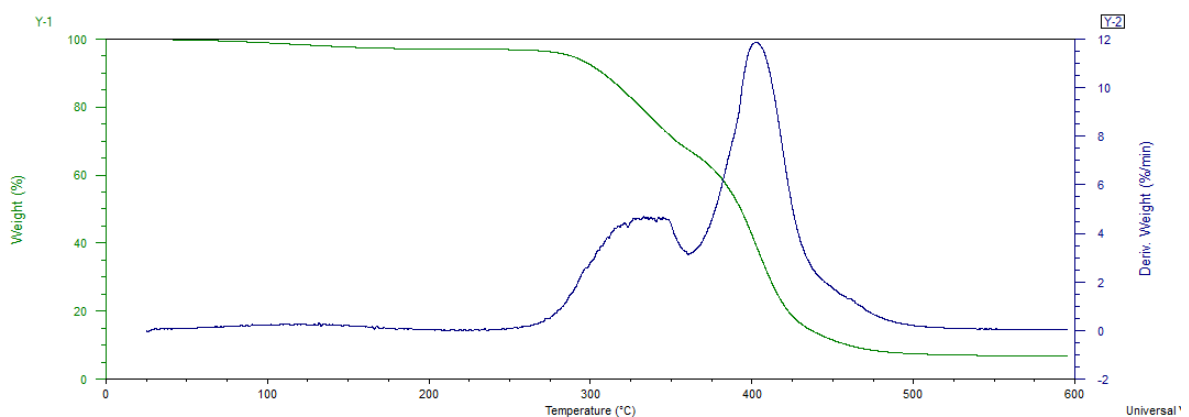


Figure 4.5 – Thermogravimetric (TGA) and TGA derivative (DTG) profiles of FOMM®-60.

No previous study was found as comparison for the FOMM[®]-60 results obtained. The material exhibited two stages of degradation, the first between 250 and 325 °C and the second between 375 and 425 °C. The DTG profile represents two reactions: the first at 330°C that occurs slowly and followed by another at 415°C, which is quicker. The Figure 4.5 can be related to the urethane thermogravimetric profile, as the decomposition of the urethane bond starts at about 220°C and forms primary amine or secondary amine and carbon dioxide. Another common behavior of urethane is weight loss around 400 °C due to degradation of the remaining structure segments, which can also be seen in the Figure 4.5 (63). As the extrusion of both materials took place at a temperature lower than 250 °C, the material processing in the 3D printer did not have influence in the thermal stability of both HIPS and FOMM[®]-60. The main thermal characteristics of the HIPS and FOMM[®]-60 filaments were studied by DSC (Figures 4.6 and 4.7). The midpoints between the beginning and shift spots of the transition temperature were chosen as the glass transition temperature (T_g) values.

For the HIPS filaments, a single thermal event was identified as the T_g of about 96°C, which fits the range of temperatures already described in a prior study (64). The DSC analyses in addition to the TGA, FTIR and water swelling tests showed that the HIPS material evaluated in the current study is the same as previous studies, making the researches comparable.

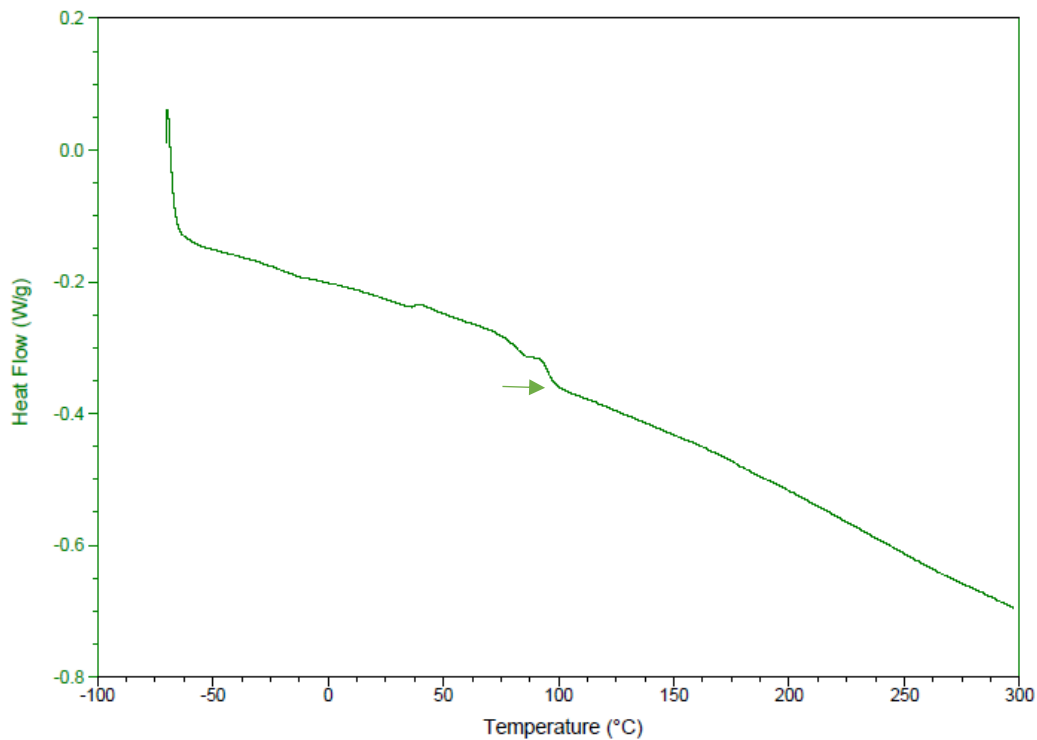


Figure 4.6 – DSC thermograms for HIPS sample with exothermal events oriented up.

FOMM[®]-60 materials thermal properties were compared among the different steps (FOMM[®]-60 as a filament, as a printed object and washed printed object) obtained through the study by DSC. The Figure 4.7 represents the DSC thermograms for FOMM[®]-60 washed samples analyses. Three thermal events were identified as endothermic valleys for this filament. The first glass transition temperature (T_{g1}) was about -30 °C and the second glass transition temperature (T_{g2}), about 5 °C. The last endothermic event represents the melting temperature (T_m), of about 120 °C. Other DSC measurements were taken for the FOMM[®]-60 as a filament and as a printed object and they can be seen in Appendix A, the figures comparison shows that the material's extrusion changes its thermal characteristics, even if there are no material degradation.

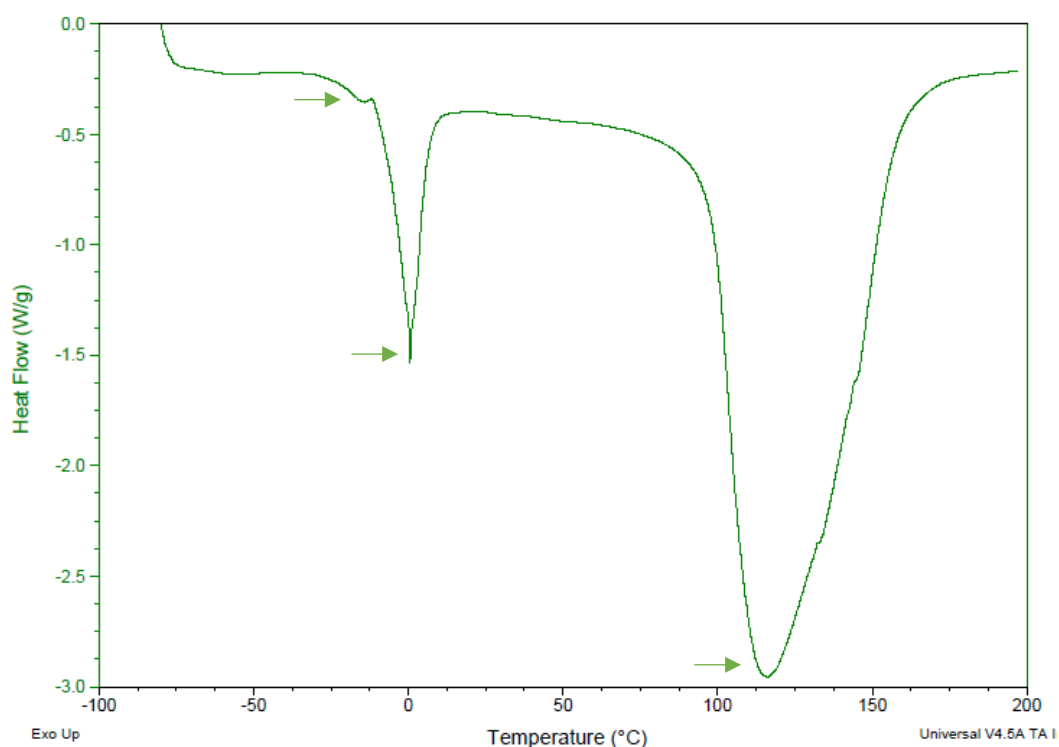


Figure 4.7 –DSC thermograms for FOMM[®]-60 sample with exothermal events oriented up.

There were no prior studies to compare FOMM[®]-60 data of this work with. Thus, the DSC thermograms for FOMM[®]-60 were compared as the polyurethane ones, once by studying the FTIR of the FOMM[®]-60 samples it was identified that the material could be composed of classic polyurethane. Yet, it was considered that PVA was not part of the polymer chain, once it was previously washed off.

Polyols are commonly used to form the polyurethane and its —OH-terminated compound display a poor thermal stability. Previous studies showed that polyurethanes have glass transition (T_g) temperatures between -40 and 34 °C. The purer the polyurethane is the lower is the temperature of its thermal events (T_g around -40 °C). The incorporation of functional groups to the polyol chain may change the value of T_g , once it interacts with other chains producing melting peaks. Therefore, the base polymer is important to define the polymeric chain thermal stability. Flexible chains, such as those of PPO (poly 2,6-dimethyl-1,4-phenylene oxide), widely used to form polyurethane, contribute to small molecular motions better than the aromatic lignin, decreasing the T_g rate. Thus, depending on the base polymer, the polyurethane present in FOMM[®]-60 may have a higher or smaller T_g and T_m values (58; 65; 66; 67; 68). As the T_g and T_m values related to the endothermic events of the

sample are different from pure polyurethane thermal properties shown by previous studies, it indicates that the analyzed FOMM[®]-60 is a copolymerized material. However, complementary studies must be carried out to complete and improve the analyses of the material.

In order to compare the results with previous studies, the TGA, DSC, FTIR and water swelling tests were used as an attempt to identify the FOMM[®]-60 components to predict the material interaction with oil and water. Although the tests carried out so far have shown a trend in the behavior of the material and some of its chemical chains, they have not revealed what it is actually made of.

4.4. Morphological analysis

The morphology of the FOMM[®]-60 sample was studied to verify if the soaking process had fulfilled the PVA extraction by the samples surface visualization. The comparison between the FOMM[®]-60 SEM analysis of the printed samples and the washed printed samples (Figure 4.8) revealed changes in the morphology of the material. Relating the SEM study to those of FTR and water swelling capacity, probably the higher porosity seen was created by the PVA leaching from the FOMM[®]-60 matrix. The pore formation enounces that there was removal of material (PVA) in these spots. This is a recurrent behaviour of FOMM[®]-60 materials and the great benefit of using this type of material is its low price associated with a material that can have its properties easily changed after the PVA removal process (69). Another factor evidenced by SEM analysis is that the porosity and roughness of the material increased after the polymer removal process. The PVA had a softening feature in the analyzed material.

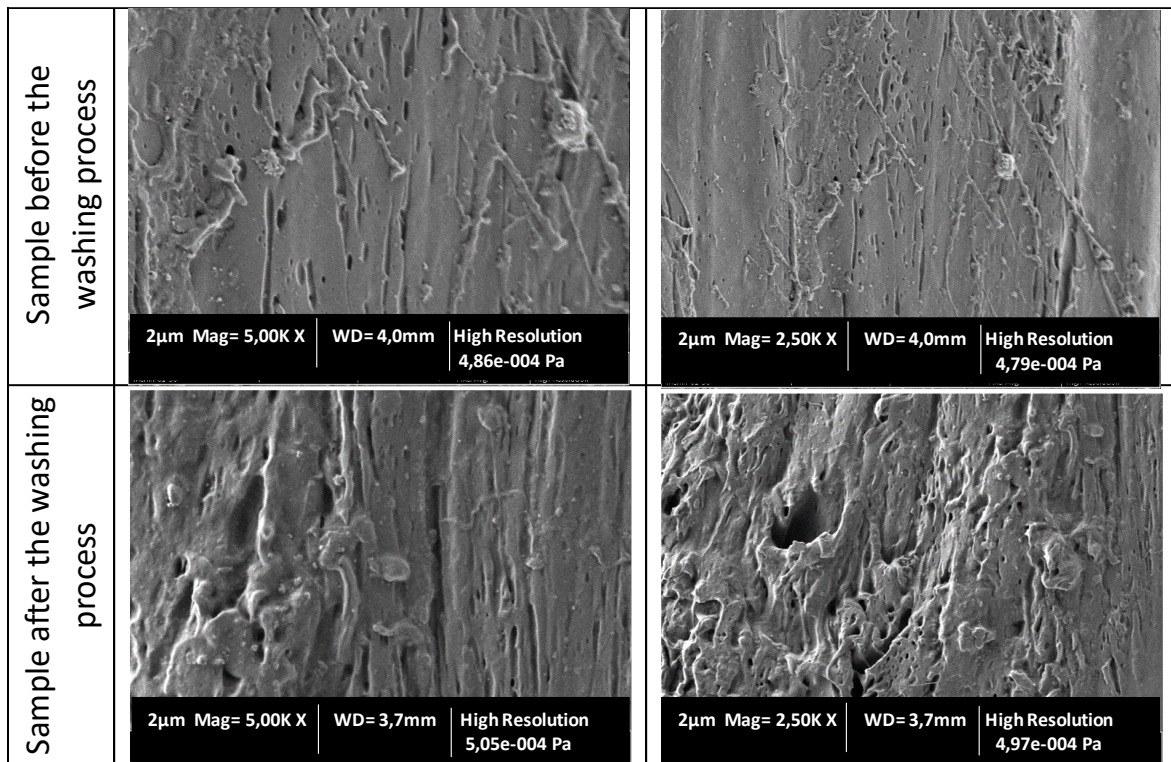


Figure 4.8 - SEM micrographs of FOMM[®]-60 samples after and before washing procedures.

4.5. Wetting of the printed samples

4.5.1. Geometrical samples

4.5.1.1. Preliminary studies

A prior study was developed with the geometrical samples, with the aim to understand how the samples' geometry, material and roughness would interfere on its interaction with drops of water and oil separately. All sample's surfaces were aligned with the horizontal (Figure 4.9) to allow the right measurement of the contact angles and the droplets were dripped with a pipette.

Figures 4.10 and 4.11 show how the contact angle of each sample varies as the drop's content is changed. The data analysis revealed that the roughness effect controlled by the print quality did not show a significant effect on the contact angles obtained (ANOVA, $P > 0.05$). However, comparing the chemical nature of both materials (FOMM[®]-60 and HIPS) in the same geometry and roughness, the chemical nature has a significant effect on

the contact angles (ANOVA, $P < 0.05$). Therefore, in the ensuing analysis, only samples with DQ roughness were printed and analyzed, since there was no noticeable change when using a different roughness.

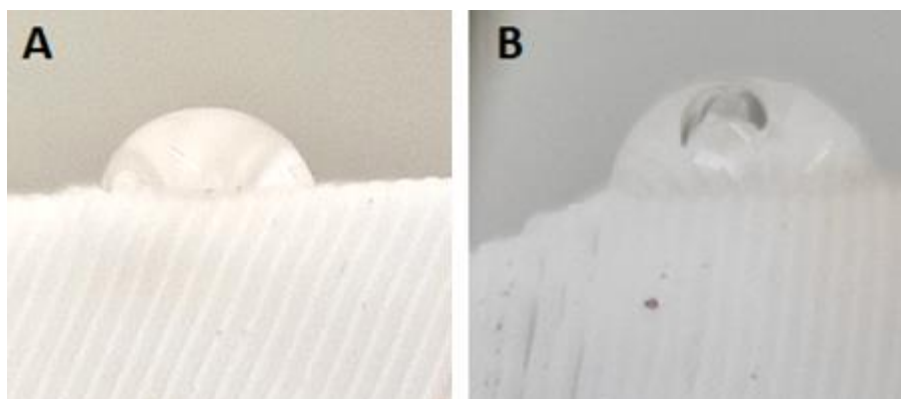


Figure 4.9– Sample’s interaction with a drop of water during the contact angle test. A) Pyramidal HIPS DQ sample B) Half sphere HIPS DQ sample.

This observation may be justified based on a previous study that show that the substrate roughness must be too small to interfere in the contact angle between its surface and the droplet. It is the case of Zhang et al. (32), whose roughness comparison shows that the presence of nanostructures results in a substantial increase in the contact angle, while the presence of microstructures does not lead to any difference in the contact angle value

The geometry effect of the printed samples has had a significant influence on the obtained contact angles for water and oil. (ANOVA, $P < 0.05$). For this reason, this study focused on repeatedly changing sample geometry and material during droplet contact angle measurement to assess wettability and the interaction among substrates. A likely reason for this behavior is that the droplets were easily captured by the surface grooves when the geometry was pyramidal, even been drained by it, as the droplets have more contact with the hierarchical surface when the sample display this type of geometry (29).

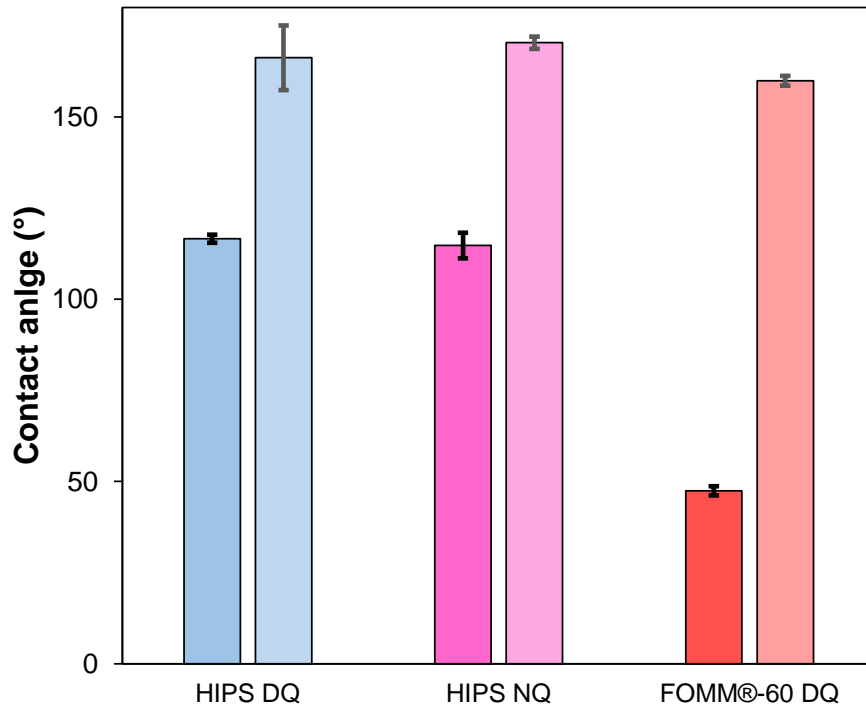


Figure 4.10 – Pyramidal samples contact angle measurement with water (■, ■) and oil (■, ■) as the drop's content.

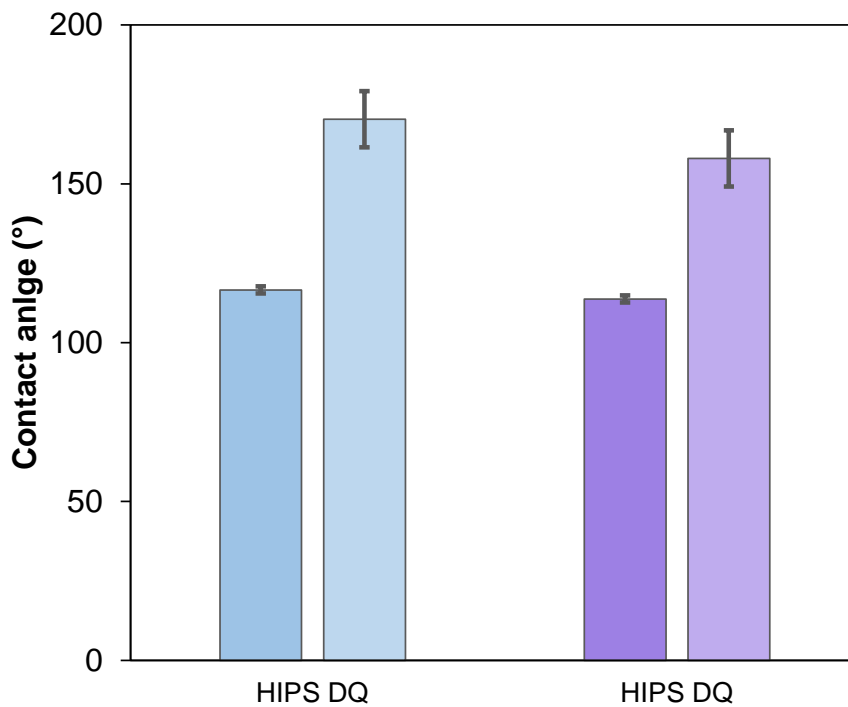


Figure 4.11 – Contact angle measurement with water and oil as the drop's content in pyramidal (■, ■) and half sphere (■, ■) samples, respectively.

4.5.1.2. Wettability analyses

This study evaluates the influence of the material surface and geometry on contact angle and wettability by dripping drops onto each one of the studied pyramidal and half sphere samples surfaces to obtain the contact angles, using instead of a pipette, an Optical Tensiometer – Teta topography equipment.

The first step of contact angle analyses carried out is shown in Figures 4.12 and 4.13. The comparison between the contact angle values reveals that the material used is significantly relevant to interfere in the interaction between the samples surface and the water and oil drop (ANOVA, $P < 0.05$). Yet, if the sample is made of FOMM[®]-60 material and the drop content is oil, the sample's geometry is also significantly relevant to interfere in this interaction (ANOVA, $P < 0.05$). The other scenarios evaluated have no significant interference of the material or geometry in the measurement of the contact angle (ANOVA, $P > 0.05$). Among them, there are the effect of geometry and material for water droplets.

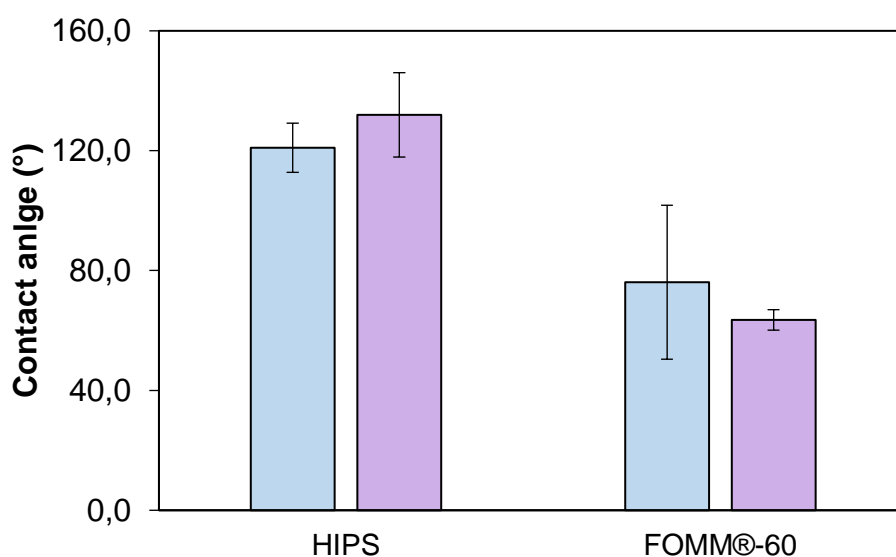


Figure 4.12 – Effect of geometry and chemical nature of printed samples on contact angles in water. Pyramidal (■) and half sphere (■) geometry, respectively.

The second step of contact angle analyses considers the Wenzel's model, which predicts that all materials display some level of roughness that affects the surfaces wettability

and therefore the final contact angle value. According to this theory, it is necessary to correct the value obtained by the parameter r_w , which is the roughness ratio between the real and the ideal solid surface zone ($r_w = 1$ if it is a smooth surface and > 1 if it is rough). While the equipment performs the analysis of the topography and contact angle, it obtains a 3D roughness parameter and r is calculated from this parameter (70).

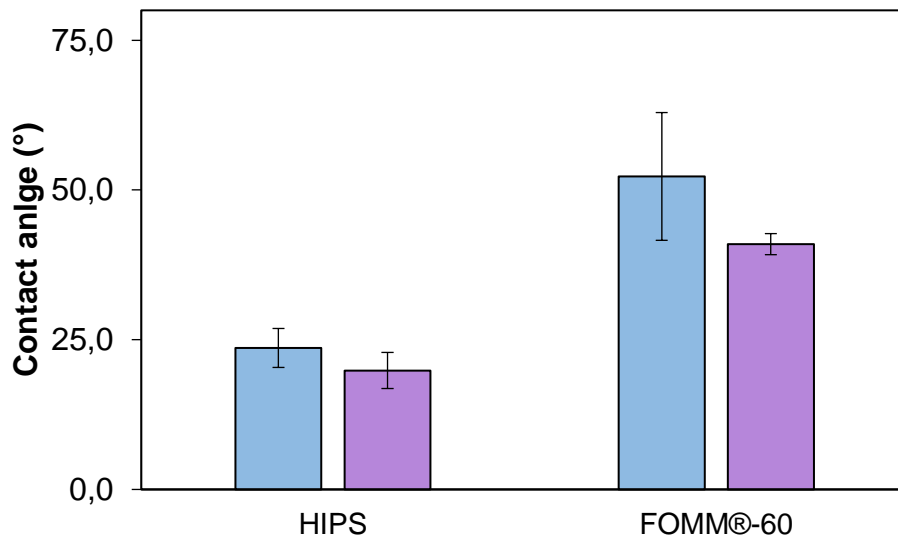


Figure 4.13 – Effect of geometry and chemical nature of printed samples on contact angles in oil. Pyramidal (■) and half sphere (■) geometry, respectively.

The values of the apparent contact angles (θ^*) of the samples when in contact with water drops are shown in Figure 4.14 and were determined using the Equation (1.2). The contact angle with roughness correction is only valid for samples in which the water droplets remain stable on the surface. Therefore, hydrophobic surfaces. Among the analyzed cases, only samples with HIPS material in contact with water drops can have the contact angle corrected, since samples with FOMM®-60 material, when in contact with water drops, absorb them. Both materials tend to absorb oil drops over time, so the contact angles between these surfaces and oil drops are considered unstable and cannot be corrected.

The data analysis indicates that neither the material or geometry exchange is significantly relevant to interfere in the interaction between the samples surface and the water drop (ANOVA, $P > 0.05$). Also, for the FOMM®-60 samples, the geometry has significant influence in the contact angle values obtained (ANOVA, $P < 0.05$).

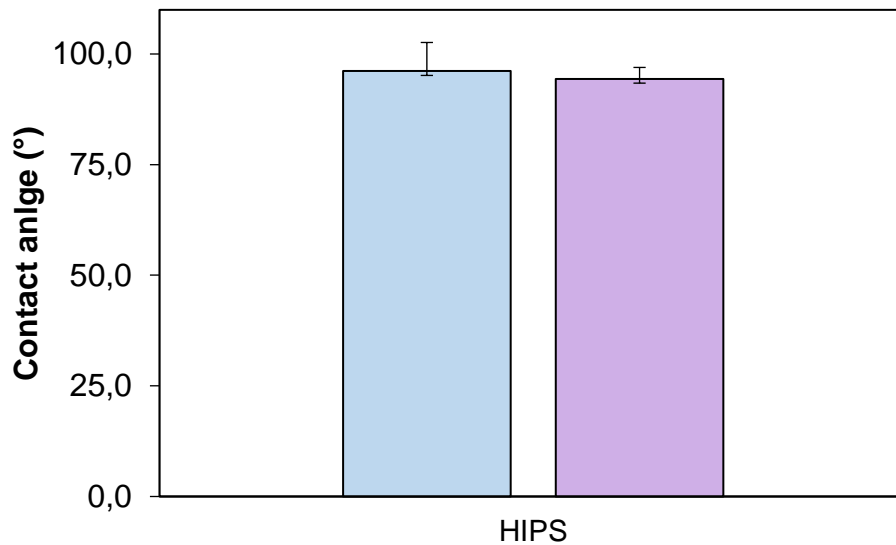


Figure 4.14 – Contact angle with correct factor r measurement with water as the drop's content in pyramidal (■) and half sphere (■) samples, respectively.

The material and geometry features show a divergent relevance regarding the contact angle between samples surfaces and water drops in both first and second steps analysis. However, in both steps the interaction HIPS material with water led to the same conclusion: the geometry is not relevant for obtaining the contact angle values.

Besides the FOMM[®]-60 is a hydrophobic material, the difference that would make it less hydrophobic than the HIPS material is due to polar chemical chains present in its composition. Furthermore, comparing samples with pyramidal and square geometry, the pyramidal increases the energy state of the surface, and thus the repellency of water droplets (the contact angle between the droplet and the surface) (71). The pyramidal geometry in the FOMM[®]-60 increases the energy state of the surface, since it leads to a bigger droplet repellency (more hydrophobic), overcoming the influence of the polar groups present in the FOMM[®]-60 material. As for HIPS, there is no significant difference as the material is already very hydrophobic.

Tables 4.3 and 4.4 show the contact angle values (with and without correction), the correction factor r and the roughness parameters (S_a , S_q). The proximity of S_a and S_q values among the samples is remarkable, excluding the pyramidal FOMM[®]-60 sample, whose parameters extrapolate the study midline observed. Once the roughness is almost

established as a standard with 3D printing, using a correction factor would not be appropriate in this circumstance. Thus, instead of correcting it, the factor r could lead to an error in the final value of the contact angle. Therefore, the contact angle values considered correct for the study were those obtained without the correction factor r in step one, although the analysis of the result lead to the same conclusion.

Table 4.3 – Water drop and surface Contact Angle Mean (CAm), standard deviation (S), Contact Angle Mean (CAm) with corrector factor and standard deviation (S) with corrector factor r , the corrector factor r and the roughness parameter (Sa and Sq).

Material	Shape	CAm	S	CAm (factor r)	S (factor r)	factor r	Sa	Sq
HIPS	Pyramidal	121,0	8,2	96,2	6,4	3,4	24,2	33,1
HIPS	Half sphere	132,0	14,1	94,4	2,5	5,0	31,1	37,1
FOMM®-60	Pyramidal	76,1	25,7	-	-	-	42,3	48,7
FOMM®-60	Half sphere	63,5	3,4	-	-	-	31,9	38,8

Table 4.4- Oil drop and surface Contact Angle Mean (CAm), standard deviation (S), and the roughness parameter (Sa and Sq).

Material	Shape	CAm	S	Sa	Sq
HIPS	Pyramidal	23,6	3,3	29,1	36,0
HIPS	Half sphere	19,9	0,4	25,6	30,5
FOMM®-60	Pyramidal	52,3	10,7	26,3	31,0
FOMM®-60	Half sphere	41,0	1,8	30,1	37,7

Even though it is not used for the analysis of the significance of the interaction between surface and droplet, Tables 4.3 and 4.4 associated with Table 4.5 and 4.6 are valuable to understand the samples hydrophobicity. Considering this, the HIPS samples exhibit a more hydrophobic character and the FOMM®-60 a more hydrophilic one.

Table 4.5 – Shape of water dropped on pyramidal and half sphere FOMM®-60 and HIPS samples.









Material	Sample's geometry	
	Pyramidal	Half sphere
FOMM®-60		
HIPS		

Table 4.6– Shape of oil dropped on pyramidal and half sphere FOMM®-60 and HIPS samples.

Material	Sample's geometry	
	Pyramidal	Half sphere
FOMM®-60		
HIPS		

4.5.1.3. Slippery test analyses

The slippery test was performed in order to better understand the samples' wettability and the dropper's adhesive characteristics in different geometries. These interactions are shown in Tables 4.7 and 4.8.

For both HIPS and FOMM®-60 samples, chemical nature affected the water droplets slip, regardless of geometry. The printed FOMM®-60 samples absorb quickly the

drops that reach the surface. What happens due to the molecule's polar bonds. Meanwhile, the printed HIPS samples repel instantly and grabs this drop. Very non-polar hydrocarbon bonds are responsible for this repellency behavior, as frictional forces prevent the fully repelled droplet from rolling down. However, a larger volume of water droplet on the HIPS surface overcome this force, leading to the droplet roll off.

The oil drops spread off the HIPS samples surface easily. There is also a tendency of the oil dropped to spread along the FOMM[®]-60 samples, but slower. This fact is observed since both materials have a good interaction with oil, though the FOMM[®]-60 material has a hydrophilic character, due to the presence of polar chemical chains and non-polar mentioned above, the material is less hydrophilic than the HIPS one. Thus, instead of repelling the solution, the material provides its spreadability along the surface.

Table 4.7– Shape of water dropped during the slippery test on pyramidal and half sphere FOMM[®]-60 and HIPS samples.


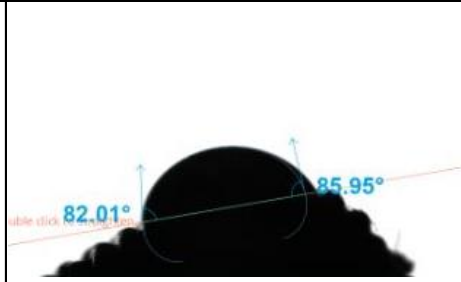

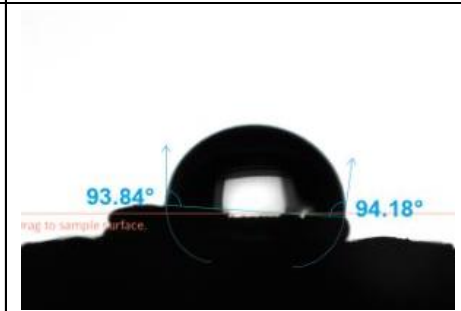

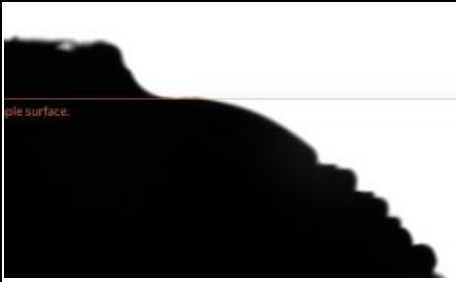
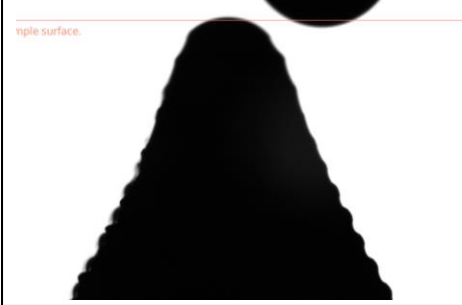
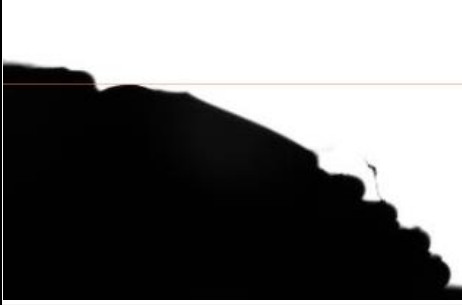
Material	Sample's geometry	
	Pyramidal	Half sphere
FOMM [®] -60		
HIPS		

Table 4.8– Shape of oil dropped during the slippery test on pyramidal and half sphere FOMM[®]-60 and HIPS samples.

Material	Sample's geometry	
	Pyramidal	Half sphere
FOMM [®] -60		
HIPS		

4.5.2. Permeable membrane samples

In the literature reviews most of the promising studies are on suspension separation process carried out using membranes, so the relationship between the surface of porous HIPS and FOMM[®]-60 membranes and oil and water were also explored. In this study, it was evaluated how the infill and material switch of these membranes can be relevant to the oil and water separation process. The 50% infill samples were compared by the infill shape (triangular and hexagonal), material (HIPS and FOMM[®]-60) and the way the drop interacts with the sample in three different moments: before the drop, the exact moment when the drop touches the material and a minute after the drop (Table 4.9).

HIPS samples with 50% of both triangular and hexagonal infill displayed the same behavior once in contact with drops of water. The drop got located above the sample's pores and did not fade away over time or get through the membrane, showing the

hydrophobicity of the HIPS material. The interaction between oil drop and samples is high in both geometries, as the drop spreads quickly along the infill and inside the pores. Another feature that allows the characterization of the HIPS material as oleophilic is the low appearance of liquid on the samples, which induces its absorption by the material. However, besides the samples that were in contact with oil drops exhibit similar performance, the triangular infill geometry allows greater dissipation of liquid than the hexagonal one. Thus, the geometry influences the interaction of the material with the oily liquid.

The FOMM[®]-60 samples with 50% of both triangular and hexagonal infill displayed a similar behavior once in contact with drops of water, as the drop fades slowly inside the pore. However, the drop dissipates more along the sample if the infill geometry is triangular. Another changing characteristic is the size of the wet area of the triangular geometry material throughout time, which is bigger than the hexagonal one. The same samples after getting in contact with oil droplets present a rapid dissipation lengthways to infill and inside the pore. The triangular shape infill pore gets emptier as time goes by, which shows that this kind of shape allows more absorption of the oil than the hexagonal one.

The HIPS and FOMM[®]-60 samples with 25% of both triangular and hexagonal infill presented pores too large compared to the liquid drop volume used during the test, considering a drop volume of 10 μ . This feature made the content pass through the mesh, not allowing the material to interact with it. However, for a larger droplet volume, the same effect that the 50% infill has for the smaller volume droplets is observed.

Table 4.9– Interaction between HIPS and FOMM®-60 samples with 50% of triangular and hexagonal infill and drops of water and oil at the moments: before the drop, the exact moment when the drop touches the material and a minute after the drops.

TIME	BEFORE THE DROP	THE ZERO TIME OF THE DROP	1 MINUTE AFTER THE DROP
FOMM®-60 - Infill 50%	PYRAMID / OIL		
	HEXAGON / OIL		
	PYRAMID / WATER		
	HEXAGON / WATER		
HIPS - Infill 50%	TRIANGLE / OIL		
	HEXAGON / OIL		
	TRIANGLE / WATER		
	HEXAGON / WATER		

Oil droplets presented a rapid dissipation lengthways to infill and inside the pores. The triangular shape infill pores get emptier as time goes by, showing that this kind of shape allows more absorption of the oil than the hexagonal one.

This study may be compared with Morgan and Gordon (72) study, which shows that the geometry of rocks as well as the pore size affect the permeability of oil/water suspensions. Meanwhile, another study may be also interesting to understand the hypothesis raised in the present work that the analyzed mesh triangular pore dispersed and retained the oil better than the hexagonal one. Klemm, Otto, et al (73) study analyzed a fog collector with pores. It basically focuses on hydrophilic material switch and its interaction with the water. The most used fog collector model around the world is the Raschel mesh, for being the one that best captures water from the environment, retaining it inside. The pores of a Raschel mesh are membranes with a triangular and 50% or higher infill (74).

CONCLUSIONS AND FUTURE WORK

The goal of this study was to verify the possibility of using the 3D printing technique to manufacture objects that separate oil and water from a mixture of both. This separation depends on the wettability of the surface by oil and water drops and it is evaluated by the contact angles. The greater the interaction, the greater the probability of separation. Simultaneously, the hypothesis of using different polymeric materials was also studied.

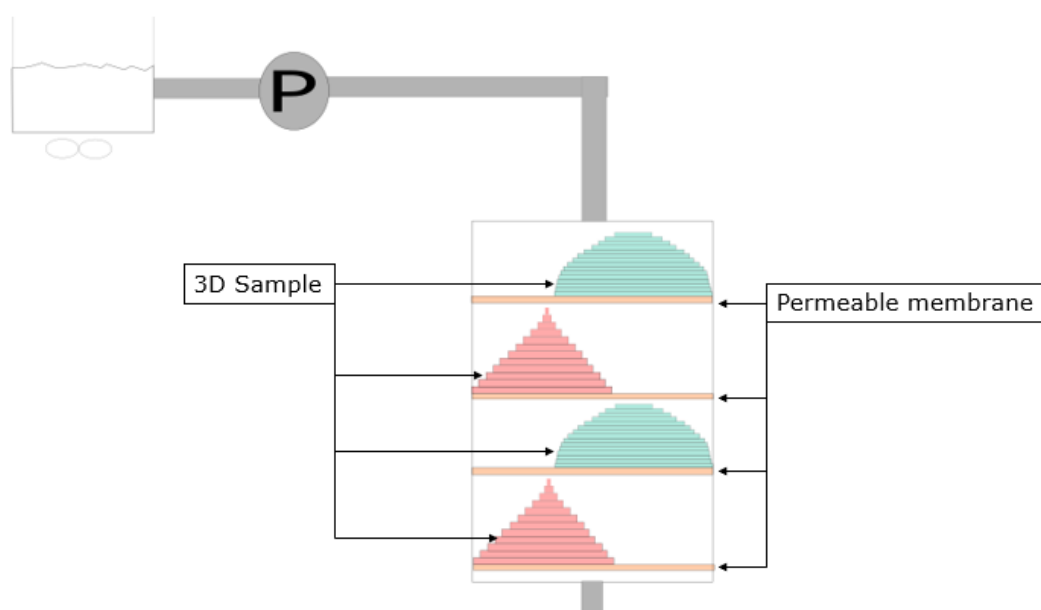
Thus, samples were printed with two different polymeric materials (HIPS and FOMM[®]-60). Other parameters were also studied: printing quality (DQ e NQ), geometry/shape (pyramidal, half sphere and permeable membrane) and porosity (triangular and hexagonal infill and 25% e 50% density). The influence of these parameters on the contact angle values was evaluated. The main conclusions of the work developed here are summarized in the following points:

- Stable materials with different chemical natures, geometry and roughness could be obtained by 3D printing;
- The roughness effect controlled by the print quality did not have any influence in the contact angle values;
- The chemistry of the polymers affects the interaction between the surface and water and oil droplets. Also, the geometry effect of FOMM[®]-60 materials is relevant to the interaction between the surface and oil droplets;
- The HIPS samples exhibit a more hydrophobic character and the FOMM[®]-60 a more hydrophilic one, when comparing both materials. However, FOMM[®]-60 samples interaction (contact angle values) with both oil and water are similar;
- The slipping test shows that both oil and water roll off drops depends on the sample geometry, material and drop volume;
- The permeable membrane samples wettability test shows that the assay with water drops reveals a bigger repelling interaction between droplet and surface. However, triangular 50% infill permeable membrane dispersed the oil and then retained it slowly and better than the hexagonal one. This oil retaining has a bigger volume for the HIPS material than the FOMM[®]-60. The geometry of the HIPS samples only interferes in the interaction

between surface and oil drop. Also, the water drops are absorbed slowly inside the FOMM[®]-60 permeable membrane pore. However, the oil drop dissipates better along the FOMM[®]-60 sample if the infill geometry is triangular;

- The samples with the greatest separating oil and water potential are the pyramidal FOMM[®]-60 and triangular 50% FOMM-60 permeable membrane, as they display parameters that are relevant to improve the wettability of the materials and the separation process.

Considering the obtained results, it would be interesting to evaluate some subsequent studies proposals. One of them is aimed to create a system that would improve the permeable membrane and 3D samples individual capacity to separate oil and water. This system is illustrated in Scheme 1. It would include an agitated alimentation of an oil/water suspension pumped through a tube, that would reach a disposal made by an association between the 3D and flat samples. The table exemplifies the distribution of the samples on side and top view. The displays emphasize that it must have a change in the position of both samples along disposal scheme.

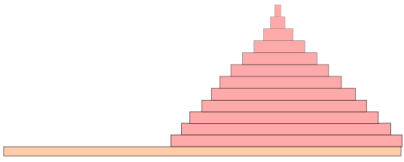
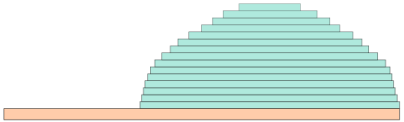
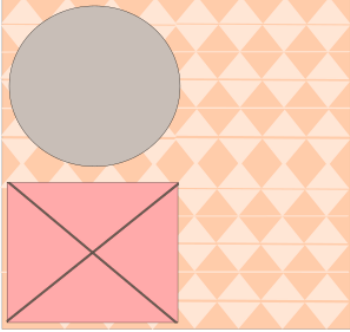
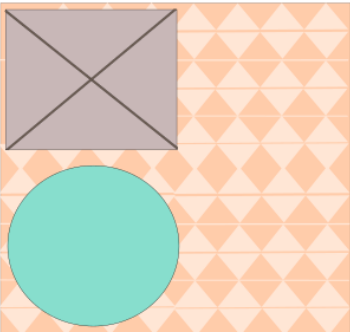


Scheme 1 – Separation process scheme with detailed distribution and position of samples and mesh on the separation disposal.

Some methods are indicated to evaluate the separating capacity of the system. Among them, it would be interesting to test physical mixtures of oil/water in different mass

proportions, (i.e., 75:25 50:50 and 25:75) and analyse the process with different oil/water flow rates, once it is controlled by a peristaltic pump.

Scheme 2 – Separation disposal distribution and position of samples and mesh on side and top view.

System	Pyramidal sample	Spheric sample
Side view		
Top view		

The flow rate could be obtained from Cycles of water harvesting effect. The technique analyses how hydrophobic is the studied structure, by heating it after each separation step in order to evaporate the water and burnout the oil. This process evaluates the presence or absence of water in the sample after the mixture flow passes through it.

BIBLIOGRAPHY

1. **R.M. Boom, Ir. A. van der Padt.** Membrane emulsification – process principles. *J. Membrane Sci.* 2003, pp. 7-8.
2. **F. Brouillet, J. Bullón, A. Cárdenas, J. Sánchez, G. Martí-Mestres, M.I. Briceño.** Modification of the droplet size and distribution of parenteral emulsions by tangential microfiltration. *Journal of Membrane Science* 221. 2003, pp. 199–206.
3. **Tescarollo, Iara Lúcia, et al.** Proposta para avaliação da qualidade de sabão ecológico produzido a partir do óleo vegetal residual. *Revista Eletronica em Gestão, Educação e Tecnologia Ambiental.* dezembro 2015, pp. 871-880.
4. **Lopes, Ana Carla Diogo.** Estudo da remoção de óleos emulsionados de efluentes industriais. *Faculdade de Engenharia da Universidade do Porto.* novembro 1999.
5. **Y. Yamashita, R. Miyahara, K. Sakamoto.** Chapter 28 - Emulsion and Emulsification Technology. *Cosmetic Science and Technology.* 2017, pp. 489-506.
6. **Y. Assadi, M.A. Farajzadeh, A. Bidari.** 2.10 - Dispersive Liquid–Liquid Microextraction. *Comprehensive Sampling and Sample Preparation.* 2012, pp. 181-212.
7. **Moreno, Eliseo Avella , et al.** Liquid–Liquid Continuous Extraction and Fractional Distillation for the Removal of Organic Compounds from the Wastewater of the Oil Industry. *Water.* 2019, pp. 1452-1468.
8. **R. Smith, M. Jobson.** Distillation. *Encyclopedia of Separation Science.* 2000, pp. 84-103.
9. **Wai, Mun Mun, et al.** Optimization and characterization of magnetite–reduced graphene oxide nanocomposites for demulsification of crude oil in water emulsion. *RSC Advances.* 2019, pp. 24003–24014.
10. **D. Möbius, R. Miller.** Chapter 5 - Examples of the implementation of hydrophilicity-lipophilicity concepts in the development of the formulations of surfactants and selection of solid particles for certain purposes. *Studies in Interface Science, Volume 9.* 2000, pp. 314-373.
11. **Rosa, D. S., Salvini, V. R. and Pandolfelli, V. C.** Processamento e avaliação das propriedades de tubos cerâmicos porosos para microfiltração de emulsões. *Cerâmica, São Paulo* , v. 52, n. 322. junho 2006, pp. 167-171.
12. **Doshi, Bhairavi, Kalliola, Simo and Sillanpää, Mika.** A review of bio-based materials for oil spill treatment. *Water Research Volume 135.* May 2018, pp. 262-277.
13. **Chen, Chaolang, et al.** Separation Mechanism and Construction of Surfaces with Special Wettability for Oil/Water Separation. *ACS Applied Materials & Interfaces.* 2019, pp. 11006-11027.
14. **Yong, Yang, et al.** Robust membranes with tunable functionalities for sustainable oil/water separation. *Journal of Molecular Liquids* 321. 2020, pp. 114701-114799.
15. **J.L., Knowlton.** Emulsion theory. *Butler H. (eds) Poucher’s Perfumes, Cosmetics and Soaps.* 1993, pp. 535-537.
16. **Whitby, Catherine P.** 3.07 - Nanoparticles at Fluid Interfaces: From Surface Properties to Biomedical Applications. *Comprehensive Nanoscience and Nanotechnology (Second Edition).* 2019, pp. 127-146.

17. **Hamberger, Anika and Landfester, Katharina.** Influence of size and functionality of polymeric nanoparticles on the adsorption behavior of sodium dodecyl sulfate as detected by isothermal titration calorimetry. *Colloid and Polymer Science* 289(1). 2010, pp. 3-14.
18. **A. Hong, A.G. Fane, R. Burford.** Factors affecting membrane coalescence of stable oil-in-water emulsions. *Journal of Membrane Science* 222. 2003, pp. 19-39.
19. **Nikolov, A. D., Randie, M., Shetty, C. S., Wasan, D. T.** Chemical demulsification of oil-in-water emulsion using air-flotation: The importance of film thickness stability. *Chemical Engineering Communications*. 1996, pp. 337–350.
20. **Al-Shamrani, A.A., James, A., & Xiao, H.** Separation of oil from water by dissolved air flotation. *Colloids and Surfaces A: Physicochemical and Engineering Aspects*. 209, 2002, pp. 15-26.
21. *Separation of water in oil emulsions using microfiltration.* **Abolfazl Ezzati, Elham Gorouhi, Toraj Mohammadi.** 2005, *Desalination*, pp. 371-382.
22. **Cui, Z. F., Jiang, Y., & Field, R. W.** Fundamentals of Pressure-Driven Membrane Separation Processes. *Membrane Technology*. 2010, pp. 1-18.
23. **Junqiang Justin Koh, Gwendolyn Lim Jia Hao, Xin Zhou, Xiwen Zhang, Jun Ding, and Chaobin He.** 3D-Printed Anti-Fouling Cellulose Mesh for Highly Efficient Oil/Water Separation Applications. *Applied Materials & Interfaces*. 2019, pp. 13787–13795.
24. **Yang, Yang, et al.** 3D-Printed Biomimetic Super-Hydrophobic Structure for Microdroplet Manipulation and Oil/Water Separation. *Advanced Materials*, 1704912. 2018.
25. **Ren, G., Song, Y., Li, X., Zhou, Y., Zhang, Z., & Zhu, X.** A superhydrophobic copper mesh as an advanced platform for oil-water separation. *Applied Surface Science*. 428, 2018, pp. 520–525.
26. **Huhtamäki, T., Tian, X., Korhonen, J. T., & Ras, R. H. A.** Surface-wetting characterization using contact angle measurements. *Nature Protocols*. 13, 2018, pp. 1521-1538.
27. **Hansson, Petra.** Hydrophobic surfaces: Effect of surface structure on wetting and interaction forces. *Royal Institute of Technology*. 2012.
28. **Zheng, Q., & Lü, C.** Size Effects of Surface Roughness to Superhydrophobicity. *Procedia IUTAM*. 10, 2014, pp. 462–475.
29. **Kang, Beomchan, Hyeon, Jini and So, Hongyun.** Facile microfabrication of 3-dimensional (3D) hydrophobic polymer surfaces using 3D printing technology. *Applied Surface Science*, 143733. 2020.
30. **Rahimpour, Mohammad Reza and Esmailbeig, Mohammad Amin.** Chapter 6 - Membrane Wetting in Membrane Distillation. *Current Trends and Future Developments on (Bio-) Membranes*. 2019, pp. 143-174.
31. **Oliveira, Márcio Roberto da Silva.** Superfícies Super-hidrofóbicas obtidas através de microestruturas litografadas. *Escola Politécnica da Universidade de São Paulo*. 2011.
32. **Zhang, B., Wang, J., & Zhang, X.** Effects of the Hierarchical Structure of Rough Solid Surfaces on the Wetting of Microdroplets. *Langmuir*. 29 (22), 2013, pp. 6652–6658.
33. **Chu, Fukai, et al.** Construction of hierarchical layered double hydroxide/poly(dimethylsiloxane) composite coatings on ramie fabric surfaces for oil/water separation and flame retardancy. *Cellulose* 27, 3485–3499. 2020.

-
34. **Li, Xiaoyu, et al.** Hierarchical rough surfaces formed by LBL selfassembly for oil–water separation†. *The Royal Society of Chemistry*. 2014, p. 11830.
35. **N. Shahrubudina, T.C. Leea, R. Ramlan.** An Overview on 3D Printing Technology: Technological, Materials, and Applications. *2nd International Conference on Sustainable Materials Processing and Manufacturing (SMPM)*. 2019, pp. 1286-1296.
36. **Zhang, Lai-Chang, et al.** Additive Manufacturing of Titanium Alloys. *Encyclopedia of Materials: Metals and Alloys*. 2021, pp. 256-274.
37. **Dudek, P.** FDM 3D Printing Technology in Manufacturing Composite Elements. *Archives of Metallurgy and Materials*. 58(4), 2013, pp. 1415–1418.
38. **Thierry Chartier, Alexander Badev.** Chapter 6.5 - Rapid Prototyping of Ceramics. *Handbook of Advanced Ceramics - Materials, Applications, Processing, and Properties*. Second Edition. s.l. : Shigeyuki Somiya, 2013, pp. 489-524.
39. **Han, Pu, et al.** Relaxation of residual stress in fused filament fabrication part with inprocess laser heating. *Procedia Manufacturing*. 53, 2021, pp. 466–471.
40. **Singh, R.** Implant Materials and Their Processing Technologies. *Reference Module in Materials Science and Materials Engineering*. 2016.
41. **Yan, Changyou, et al.** 3D printing of bioinspired textured surfaces with superamphiphobicity. *Nanoscale*. 2020, pp. 303-306.
42. **Berczeli, Miklós and Weltsch, Zoltán.** Enhanced Wetting and Adhesive Properties by Atmospheric Pressure Plasma Surface Treatment Methods and Investigation Processes on the Influencing Parameters on HIPS Polymer. *Polymers 13, no. 6: 901*. 2021.
43. **Masood, M. T., Heredia-Guerrero, J. A., Ceseracciu, L., Palazon, F., Athanassiou, A., & Bayer, I. S.** Superhydrophobic high impact polystyrene (HIPS) nanocomposites with wear abrasion resistance. *Chemical Engineering Journal doi*. 2017, pp. 322, 10–21.
44. **Vouvoudi, Evangelia C., Rousi, Aristeia T. and Achilias, Dimitris S.** Thermal degradation characteristics and products obtained after pyrolysis of specific polymers found in Waste Electrical and Electronic Equipment. *Frontiers of Environmental Science & Engineering*. 2017, pp. 9-19.
45. **Gaaz, Tayser Sumer, et al.** Properties and Applications of Polyvinyl Alcohol, Halloysite Nanotubes and Their Nanocomposites. *Molecules*. 20(12), 2015, pp. 22833–22847.
46. **Huihua Li, Min Wang.** 18 - Electrospinning and nanofibrous structures for biomedical applications. *In Elsevier Series on Advanced Ceramic Materials, Bioceramics*. s.l. : Elsevier, 2021, pp. 401-436.
47. **Jiseon, You, et al.** 3D printed components of microbial fuel cells: Towards monolithic microbial fuel cell fabrication using additive layer manufacturing. *Sustainable Energy Technologies and Assessments*. 2017, p. 19.
48. **Preininger, Claudia and Chiarelli, Piero.** Immobilization of oligonucleotides on crosslinked poly(vinyl alcohol) for application in DNA chips. 2002, pp. 0-9.
49. **Jia, Shikui, et al.** Composites of poly(lactic) acid/thermoplastic polyurethane/mica with compatibilizer: morphology, miscibility and interphase. *RSC Advances*. 2015, pp. 98915-98924.
50. **Sanatgar, Raziieh Hashemi .** FDM 3D printing of conductive polymer nanocomposites: A novel process for functional and smart textiles. *The Swedish School of Textiles*. 2018, pp. 72011–72016.
51. **Singh, Sudarshan and Bothara, Sunil B.** Physico-chemical and structural characterization of mucilage isolated from seeds of *Diospyros melonoxylon* Roxb. *Brazilian Journal of Pharmaceutical Sciences*. 2014, pp. 713-725.
-

52. **Worsfold, Paul, Townshend, Alan and Poole, Colin.** FORENSIC SCIENCES | Systematic Drug Identification. *Encyclopedia of Analytical Science (Second Edition)*. 2005, pp. 471-480.
53. **Höhne, Günther, Hemminger, Wolfgang F. and Flammershei, H.-J.** *Differential Scanning Calorimetry*. 2003.
54. **Khare, Tushar, et al.** Biologically synthesized nanomaterials and their antimicrobial potentials. *Comprehensive Analytical Chemistry*. 2019, pp. 263-289.
55. **Farré, Marinella and Barceló, Damià.** Chapter 1 - Introduction to the Analysis and Risk of Nanomaterials in Environmental and Food Samples. *Comprehensive Analytical Chemistry, Volume 59*. 2012, pp. 1-32.
56. **Wang, Ze-Nian, et al.** Experimental investigation of water-swelling characteristics of polymer materials for tunnel sealing gasket. *Construction and Building Materials*, 256. 2020.
57. **Silva, Eliezer, et al.** Elaboração de Mini Extrusora de Escala Laboratorial: Processamento e Reciclagem de Materiais Poliméricos. *Revista Eletrônica de Materiais e Processos*, v. 15. 2020, pp. 50-53.
58. **Carvalho, Sabrina M., et al.** Caracterização de Poliuretano Baseado em Polioli Sintetizado a partir de Glicerol e Hexametileno Diisocianato. *10º Congresso Brasileiro de Polímeros*. 2009.
59. **Alhosseini, Sanaz Naghavi, et al.** Synthesis and characterization of electrospun polyvinyl alcohol nanofibrous scaffolds modified by blending with chitosan for neural tissue engineering. *International Journal of Nanomedicine*, 25. 2012.
60. **Brady, James E.** Polymer Properties and Characterization. *Developing Solid Oral Dosage Forms*. 2009, pp. 187-217.
61. **Reynolds, William F.** Polar substituent effects. [book auth.] Robert W. Taft. *Progress in Physical Organic Chemistry*. 2009.
62. **Vilaplana, Francisco, Ribes-Greus, Amparo and Karlsson, Sigbritt.** Analytical strategies for the quality assessment of recycled high-impact polystyrene: A combination of thermal analysis, vibrational spectroscopy, and chromatography. *Analytica Chimica Acta*, 604(1). 2007, pp. 18–28.
63. **Monteavaro, Luciane L., et al.** Thermal stability of soy-based polyurethanes. *Polímeros* 15. 2005, pp. 151-155.
64. **Ma, Weihua, Ding, Jie and Zhong, Qin.** Foaming of Polystyrene with Supercritical Carbon Dioxide. *Advanced Materials Research*, 669. 2013, pp. 366-370.
65. **Kelly, Stephen S., Glasser, Wolfgang G. and Ward, Thomas C.** Engineering Plastics from Lignin. XV. Polyurethane Films from Chain-Extended Hydroxypropyl Lignin. *Journal of Applied Polymer Science*. 1998, pp. 759–77.
66. **Clemente, Marcelo, et al.** Desenvolvimento de Tecnologia de Pré-Polímeros na Síntese de Poliuretanos Empregados em Combustíveis Sólidos. *Quim. Nova*, Vol. 37, No. 6. 2014, pp. 982-988.
67. **Martin, Darren J., et al.** The effect of average soft segment length on morphology and properties of a series of polyurethane elastomers. II. SAXS-DSC annealing study. *Journal of Applied Polymer Science*. 1996, pp. 803-817.
68. **Kojio, Ken, et al.** Influence of chemical structure of hard segments on physical properties of polyurethane elastomers: a review. *Journal of Polymer Research*. 2020, pp. 27-33.

69. **Li, Feng, et al.** 3D printing in analytical sample preparation. *Journal of Separation Science*. 2020, pp. 1-32.
70. **Berg, John C.** Chapter 1 - Semi-empirical strategies for predicting adhesion. *Adhesion Science and Engineering*. 2002, pp. 1-73.
71. **Gong, Wei, et al.** A Study of the Truncated Square Pyramid Geometry for Enhancement of Super-hydrophobicity. *Journal of Bionic Engineering*. 2020, pp. 843–850.
72. **Morgan, J.T. and Gordon, D.T.** Influence of Pore Geometry on Water-Oil Relative Permeability. *Journal of Petroleum Technology*. 1970, pp. 1199–1208.
73. **Klemm, Otto, et al.** Fog as a Fresh-Water Resource: Overview and Perspectives. *Royal Swedish Academy of Sciences 2012*. 2012, pp. 221–234.
74. **Rajaram, Mithun, et al.** Enhancement of fog-collection efficiency of a Raschel mesh using surface coatings and local geometric changes. *Colloids and Surfaces A: Physicochemical and Engineering Aspects*. 2012, pp. 218–229.
75. **Streb, Cleci Schaleberger , Cunha, Kamyla Borges da and Negrini, Valéria Simensato .** Reciclagem de óleos lubrificantes: solução ambiental, legal e econômica. *Congresso Brasileiro de Ciência e Tecnologia em Resíduos e Desenvolvimento Sustentável*. 2004, pp. 4301-4310.

APPENDIX A – DSC ANALYSES RESULTS FOR FOMM[®]-60 FILAMENTS

The DSC characteristic curve analysis of the FOMM[®]-60 sample for filament before 3D printing and after printing is shown in Figures A1 and A2. The comparison shows that the material's extrusion changes its thermal characteristics, even if there are no material degradation. In both analyses there are of PVA in the analyzed material.

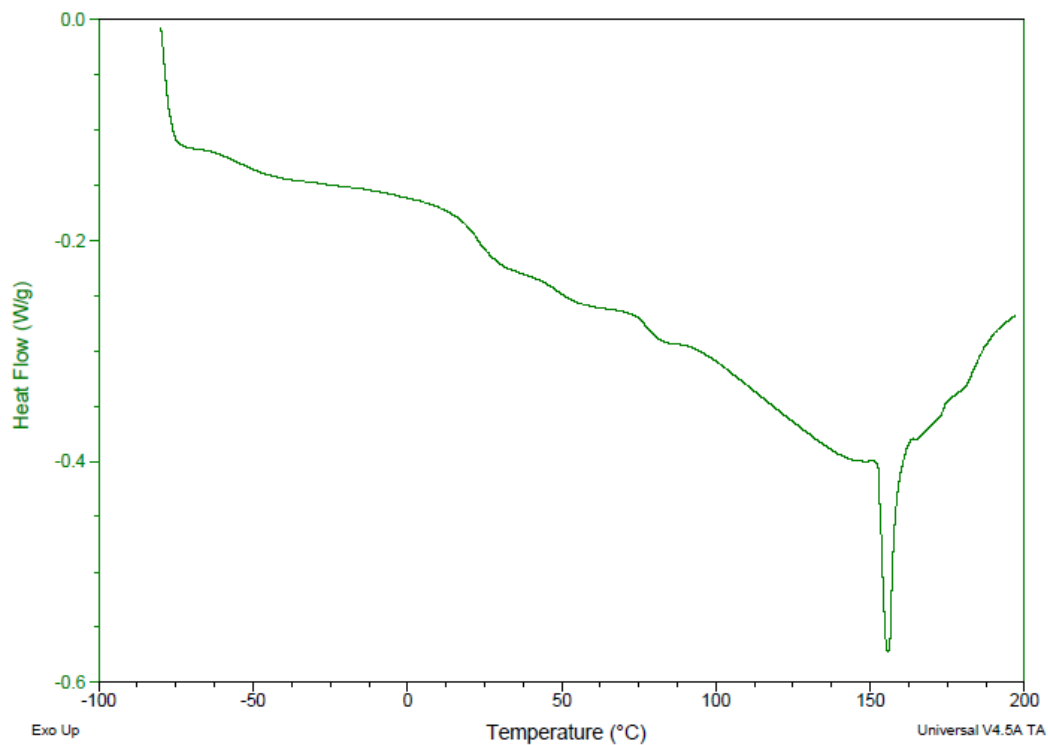


Figure A1 – DSC of FOMM[®]-60 filament before 3D printing and washing by heat flow and increase of temperature, with exothermic peaks and endothermic valleys.

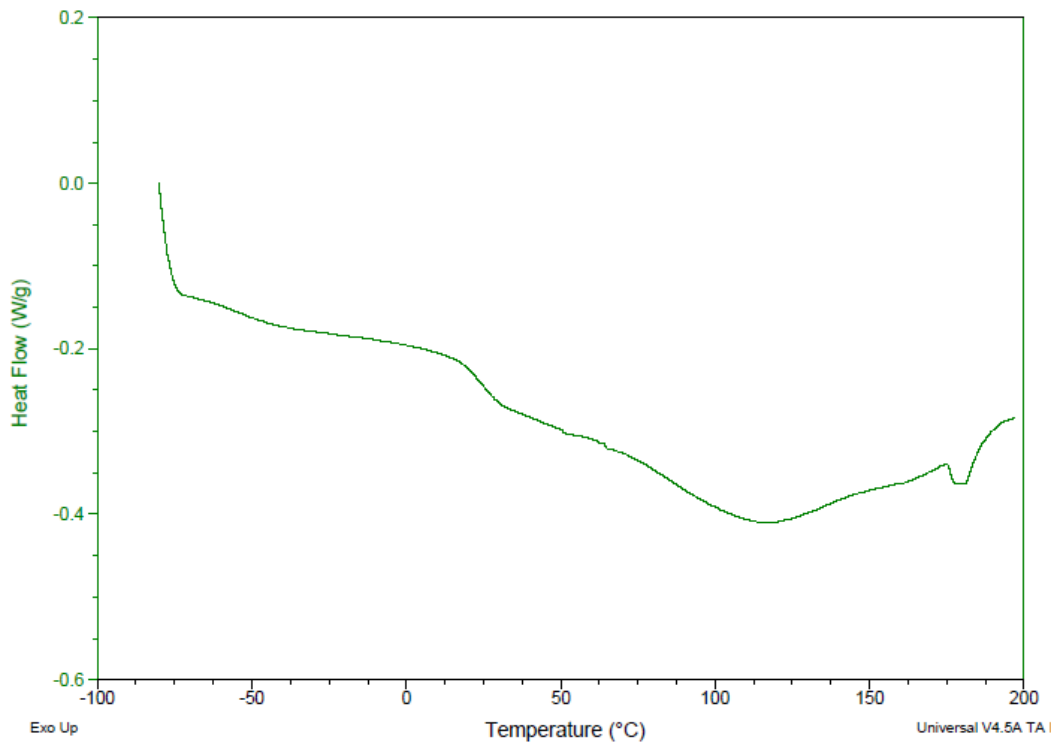


Figure A2 – DSC of FOMM®-60 filament after 3D printing and before washing by heat flow and increase of temperature, with exothermic peaks and endothermic valleys.